cmgh
CELLULAR AND MOLECULAR GASTROENTEROLOGY AND HEPATOLOGY

ORIGINAL RESEARCH

Activation of Liver mTORC1 Protects Against NASH via Dual Regulation of VLDL-TAG Secretion and *De Novo* Lipogenesis

Kahealani Uehara,[1,2] Jaimarie Sostre-Colón,[1] Matthew Gavin,[1] Dominic Santoleri,[1,2] Kelly-Ann Leonard,[3] René L. Jacobs,[3] and Paul M. Titchenell[1,4]

[1]Institute for Diabetes, Obesity, and Metabolism, Perelman School of Medicine, University of Pennsylvania, Philadelphia, Pennsylvania, USA; [2]Biochemistry and Molecular Biophysics Graduate Group, Perelman School of Medicine, University of Pennsylvania, Philadelphia, Pennsylvania, USA; [3]Department of Agricultural, Food and Nutritional Science; Department of Biochemistry, University of Alberta, Edmonton, Alberta, Canada; and [4]Department of Physiology, Perelman School of Medicine, University of Pennsylvania, Philadelphia, Pennsylvania, USA

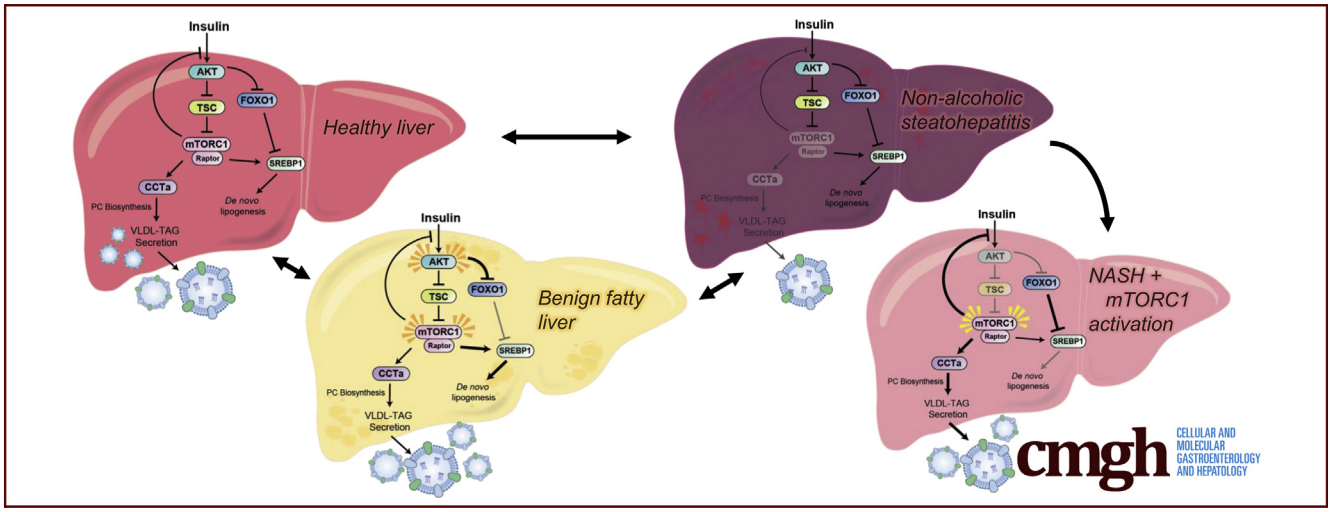

SUMMARY

Hepatic mechanistic target of rapamycin complex 1 activity is elevated in mouse models of insulin-resistant, fatty liver conditions but is decreased in mouse models of nonalcoholic steatohepatitis. Genetic activation of mechanistic target of rapamycin complex 1 in hepatocytes enhances lipid export from the liver while suppressing lipid synthesis to protect against nonalcoholic steatohepatitis.

BACKGROUND & AIMS: Dysregulation of liver lipid metabolism is associated with the development and progression of nonalcoholic fatty liver disease, a spectrum of liver diseases including nonalcoholic steatohepatitis (NASH). In the liver, insulin controls lipid homeostasis by increasing triglyceride (TAG) synthesis, suppressing fatty acid oxidation, and enhancing TAG export via very low-density lipoproteins. Downstream of insulin signaling, the mechanistic target of rapamycin complex 1 (mTORC1), is a key regulator of lipid metabolism. Here, we define the role of hepatic mTORC1 activity in mouse models of NASH and investigate the mTORC1-dependent mechanisms responsible for protection against liver damage in NASH.

METHODS: Utilizing 2 rodent NASH-promoting diets, we demonstrate that hepatic mTORC1 activity was reduced in mice with NASH, whereas under conditions of insulin resistance and benign fatty liver, mTORC1 activity was elevated. To test the beneficial effects of hepatic mTORC1 activation in mouse models of NASH, we employed an acute, liver-specific knockout model of TSC1 (L-TSC-KO), a negative regulator of mTORC1.

RESULTS: L-TSC-KO mice are protected from and have improved markers of NASH including reduced steatosis, decreased circulating transaminases, and reduced expression of inflammation and fibrosis genes. Mechanistically, protection from hepatic inflammation and fibrosis by constitutive mTORC1 activity occurred via promotion of the phosphatidylcholine synthesizing enzyme, CCTα, and enhanced very low-density lipoprotein-triglyceride export. Additionally, activation of mTORC1 protected from hepatic steatosis via negative feedback of the mTORC2-AKT-FOXO-SREBP1c lipogenesis axis.

CONCLUSIONS: Collectively, this study identifies a protective role for liver mTORC1 signaling in the initiation and progression of NASH in mice via dual control of lipid export and synthesis. *(Cell Mol Gastroenterol Hepatol 2022;13:1625–1647; https://doi.org/10.1016/j.jcmgh.2022.02.015)*

Keywords: CCTα; FOXO1; Insulin; Nonalcoholic Fatty Liver Disease; Phosphatidylcholine.

Nonalcoholic fatty liver disease (NAFLD) is now recognized as a leading cause of liver disease worldwide.[1] NAFLD is a spectrum of diseases that comprise benign fatty liver and nonalcoholic steatohepatitis (NASH), which correlate strongly with metabolic diseases such as obesity, insulin resistance, and type 2 diabetes.[2] The hallmarks of NAFLD include increased lipid accumulation in the liver, known as hepatic steatosis or nonalcoholic fatty liver (NAFL).[3] In some cases, individuals with NAFL can develop NASH, where steatosis is accompanied by inflammation, fibrosis, and cell death, which may ultimately lead to cirrhosis and liver failure.[4] Importantly, progression of NASH is associated with increased incidence of hepatocellular carcinoma and severe illnesses from viral infections such as COVID-19.[5,6]

Weight reduction, including lifestyle interventions and bariatric surgery, show promise in improving NASH pathology.[7,8] Despite this, there are currently no United States Food and Drug Administration-approved medical treatments for NASH. Therefore, detailed molecular investigation of the metabolic drivers of NAFL and NASH may uncover new therapeutic opportunities. Current research is focused on inactivation of inflammatory and lipogenic metabolic pathways.[7,9] Many ongoing clinical trials focusing on inflammation include drugs targeting chemokine receptors, thyroid hormone receptors, and farnesoid X receptors.[10-12] For example, the farnesoid X receptor agonist, obeticholic acid, completed a phase III clinical trial and modestly improved fibrosis in patients with NASH, but did not gain United States Food and Drug Administration approval due to potential safety risks and modest efficacy.[10] As a result, there remains a significant unmet need for the elucidation of the molecular drivers of NAFLD.

In addition to targeting inflammation and fibrosis modulators, the potential of antagonizing key enzymes involved in regulating hepatic lipid metabolism is of significant therapeutic interest. In particular, increased hepatic *de novo* lipogenesis (DNL) is a distinguishing feature of patients with NAFLD.[13-15] The liver is a key metabolic organ regulating lipid homeostasis by coordinating lipid synthesis, breakdown, uptake, and export.[16] In response to feeding, insulin signals to the liver to increase DNL, suppress fatty acid oxidation, and promote triglyceride (TAG) esterification to increase lipid secretion.[17] Many lipid metabolism pathways are altered in the development and progression of NAFLD.[2] Blockade of fatty acid synthetase (FASN), acetyl-coA carboxylase (ACC), or diacylglycerol acetyltransferase 2 (DGAT2), key enzymes involved in lipid synthesis, showed positive effects on reducing hepatic lipid burden and fibrosis in clinical trials of NASH.[18-20] Furthermore, agonists targeting peroxisome proliferator-activated receptors (PPAR), key regulators of lipid oxidation, improved many hallmarks of NASH without worsening of fibrosis.[21] However, these drugs are in ongoing clinical trials, and recent data revealed acetyl-coA carboxylase inhibition leads to hypertriglyceridemia[22]; thus, it is unclear whether inhibiting DNL or increasing oxidation alone will be sufficient to improve NASH.

In the liver, insulin and other growth factors activate many downstream signaling pathways to regulate lipid homeostasis. Of note, the mechanistic target of rapamycin complex 1 (mTORC1) is a critical node in the regulation of hepatic lipid homeostasis, receiving input from hormones, growth factors, and nutrients.[23] During periods of prolonged fasting, inhibition of mTORC1 is necessary for the induction of hepatic ketogenesis.[24] Postprandially, protein kinase B (PKB or AKT) is activated by insulin, which inhibits the tuberous sclerosis complex (TSC), leading to the activation of mTORC1.[25] Insulin activation of mTORC1 signaling is required, but not sufficient, for the activation of DNL, in part via regulation of the master regulator of lipogenic gene expression, sterol regulatory element binding protein 1 (SREBP1).[26,27] Paradoxically, constitutive activation of mTORC1 does not promote lipid synthesis, rather, it leads to the suppression of lipogenic transcription, due to a negative feedback regulation of the mTORC2-AKT axis.[28-32] Lastly, insulin acts through many pathways to regulate hepatic lipid export via very-low-density-lipoproteins (VLDL).[33] Although insulin is canonically known to reduce VLDL-TAG and apolipoprotein B secretion in isolated hepatocytes, hepatic insulin signaling is required for VLDL-TAG export *in vivo*.[33,34] Mechanistically, our laboratory recently demonstrated that the mTORC1-dependent control of VLDL-TAG secretion, through its promotion of phosphatidylcholine (PC) synthesis, is critical for both hepatic and circulating TAG homeostasis.[34] Thus, liver mTORC1 signaling plays an essential role in regulating both hepatic and systemic lipid metabolism.

Despite the immense effort to understand how insulin signaling controls liver lipid homeostasis, there remains a dearth of knowledge about how these signaling pathways contribute to the initiation and development of NAFL and NASH. Specifically, the direct role of mTORC1 in NAFL and NASH livers remain elusive. Current data suggest liver mTORC1 activity is elevated in mouse models of insulin-resistance and benign fatty liver, which correlate with increased DNL and VLDL-TAG secretion in NAFL.[13,35]

Abbreviations used in this paper: **AAV, adeno-associated virus; AKT, protein kinase B; ALT, alanine aminotransferase; AST, aspartate aminotransferase; CCTα, CTP:Phosphocholine cytidylyltransferase alpha; DNL, *de novo* lipogenesis; DKO, double knockout; FOXO, forkhead box O; GAN, Gubra-modified Amylin diet; HFD, high-fat diet; i.p., intraperitoneal; KO, knockout; LMCD-HFD, low methionine; choline-deficient, high fat diet; mTORC1, mechanistic target of rapamycin; NAFL, nonalcoholic fatty liver; NAFLD, nonalcoholic fatty liver disease; NASH, nonalcoholic steatohepatitis; PC, phosphatidylcholine; PCR, polymerase chain reaction; PE, phosphatidylethanolamine; SREBP, sterol regulatory-element binding protein; TAG, triglyceride; TBG, thyroxine binding globulin; TSC, tuberous sclerosis complex; VLDL, very-low-density lipoproteins.**

Most current article

2352-345X
https://doi.org/10.1016/j.jcmgh.2022.02.015

However, the role of mTORC1 in NASH is less understood. In animal models, *in vivo* inhibition of mTORC1, through deletion of hepatic Raptor protein, or through long-term rapamycin treatment, induces inflammation, fibrosis, and liver damage in mice.[36] Clinical studies using mTORC1 inhibitors did not improve overall survival of patients with advanced liver damage.[37] Furthermore, clinical studies in humans have identified a reduction in VLDL synthesis and secretion in pathology-confirmed NASH.[38] Therefore, we hypothesize that mTORC1 has a biphasic role in the development and progression of NAFLD. In this study, we test the hypothesis that reduced liver mTORC1 signaling is a key transition point for the progression of benign fatty liver to steatohepatitis.

Results

mTORC1 Activity is Differentially Regulated During the Initiation and Progression of NASH in Mice

Previous studies demonstrated an enhancement of mTORC1 activity during obesogenic, insulin-resistant, and benign steatotic conditions, such as in diet-induced obese and genetically obese rodents.[35,39,40] However, less is known about mTORC1 activity through the progression to bona fide NASH in rodents. To evaluate the role of mTORC1 through NAFLD initiation and progression, we utilized genetic and diet-induced mouse models of steatosis and steatohepatitis. In the insulin-resistant *ob/ob* mouse model, pronounced accumulation of lipid droplets was observed without indication of fibrosis (Figure 1*A*). As previously reported, phosphorylation of AKT and S6 were significantly increased upon fasting, suggesting increased insulin signaling via the AKT-mTORC1 axis under these conditions of insulin-resistance and benign fatty liver with no evidence of fibrosis (Figure 1*B*).[35,39,41]

To directly ascertain the role of mTORC1 signaling in NASH livers, we fed mice 2 distinct NASH-promoting diets. First, a cohort of mice were challenged with a high-fat, low-methionine, choline-deficient diet (45% kcal fat, 0.1% methionine, no added choline), referred to here as "LMCD-HFD."[42] LMCD-HFD-fed mice displayed prominent hepatic steatosis and collagen deposition following 4 weeks of feeding, compared with age-matched mice fed a control L-amino acid diet (10 kcal% fat with methionine and choline), as previously reported[43] (Figure 1*C*). Notably, substantial rise in inflammation and fibrotic gene expression was observed in response to LMCD-HFD-feeding (Figure 1*D*), correlating with increase in circulating transaminases, aspartate aminotransferase (AST), and alanine aminotransferase (ALT), indicators of liver damage (Figure 1*E*). The induction of liver damage, fibrosis, and inflammation paralleled a reduction of both VLDL-TAG secretion (Figure 1*F*) and hepatic mTORC1 activity, as quantified by a decrease in phosphorylated to total ratios of the mTORC1 targets, S6, and 4EBP1 proteins following a 6-hour fast (Figure 1*G*). Surprisingly, proximal signaling via AKT was not suppressed under these conditions. Rather, phosphorylation was modestly enhanced, indicating mTORC1 is reduced independent of any changes in proximal AKT activity in this NASH model (Figure 1*G*).

Next, we assessed mTORC1 activity in a dietary NASH model that does not rely on nutrient limitations. The Gubra-modified AMLN diet (40% kcal fat [mostly palm oil], 20% kcal fructose, and 2% cholesterol, Research Diets), referred to here as "GAN diet," induces NASH upon 30 weeks of feeding.[44,45] Following 30 weeks of diet administration, mouse livers displayed histological induction of fibrosis and steatosis (Figure 1*H*). Similar to the LMCD-HFD cohort, GAN diet-fed mice had reduced rates of VLDL-TAG secretion (Figure 1*I*), correlating with a reduction pS6/total S6 ratio indicating reduced mTORC1 activity (Figure 1*J and K*). Collectively, these data suggest that mTORC1 is differentially regulated during the initiation and development of NAFLD, such that in simple steatosis and insulin-resistance, hyperinsulinemia leads to increased liver mTORC1 activity. However, under NASH-like conditions, hepatic mTORC1 activity is reduced despite normal or enhanced proximal AKT signaling.

Acute mTORC1 Activation Prevents and Improves Steatosis, Inflammation, and Fibrosis in Mice on NASH Diet

To counteract the decrease in mTORC1 signaling in NASH livers, we utilized a mouse model of acute deletion of TSC1. The TSC complex negatively regulates mTORC1 activation via AKT; therefore, mice lacking TSC1 have constitutive mTORC1 activity independent of proximal AKT signaling.[46] Briefly, *Tsc1*$^{loxp/loxp}$ mice were injected with adeno-associated virus serotype 8, driven by a thyroxine binding globulin (AAV8-TBG) promoter containing either -Cre (L-TSC-KO) or -GFP (Control) 2 weeks prior to a 4-week LMCD-HFD feeding to test whether constitutive mTORC1 activity protects against diet-induced NASH (Figure 2*A*). Phosphorylation of S6 to total S6 was enhanced in L-TSC-KO mouse livers, and TSC1 protein was undetectable, confirming deletion of TSC1 and *in vivo* activation of liver mTORC1 (Figure 2*B*). Four weeks after LMCD-HFD feeding, L-TSC-KO mice displayed reduced expression of several markers of fibrosis (*Col1a1, Acta2, Pdgfb, Tgfb1, Timp1*) and inflammation (*Il1b, Ccl2, Tnf, Saa1, Adgre1*) (Figure 2*C*). Consistently, L-TSC-KO mice displayed lower plasma ALT and AST activity, suggesting an attenuation of liver damage in L-TSC-KO mice (Figure 2*D*). Gene expression changes correlated with a histological decrease in collagen deposition as documented by Sirius red staining (Figure 2*E*). Histological assessment documented an improvement in fibrosis and steatosis staging between L-TSC-KO and control mice (Figure 2*F and G*). Histological changes were accompanied by a significant decrease in TAG accumulation in the livers of L-TSC-KO mice (Figure 2*H*).

Previous work in models of both acute and chronic mTORC1 activation exhibit an anti-steatotic effect under fasting and obesogenic challenges, such as HFD feeding.[28,32,34] This phenomenon was attributed to a decrease in DNL and a parallel increase in fatty acid oxidation.[24,28] More recently, our laboratory identified a

dominant role for mTORC1 in the promotion of VLDL-TAG secretion and control of hepatic lipid accumulation.[34] Therefore, to test the specific role of VLDL-TAG secretion in our L-TSC-KO NASH model, we injected fasted L-TSC-KO mice with poloxamer-407 (p407) detergent, a compound that blocks lipoprotein lipases, and measured TAG secretion as the accumulation of TAG in the blood over time.[47] Constitutive mTORC1 activation increased TAG secretion

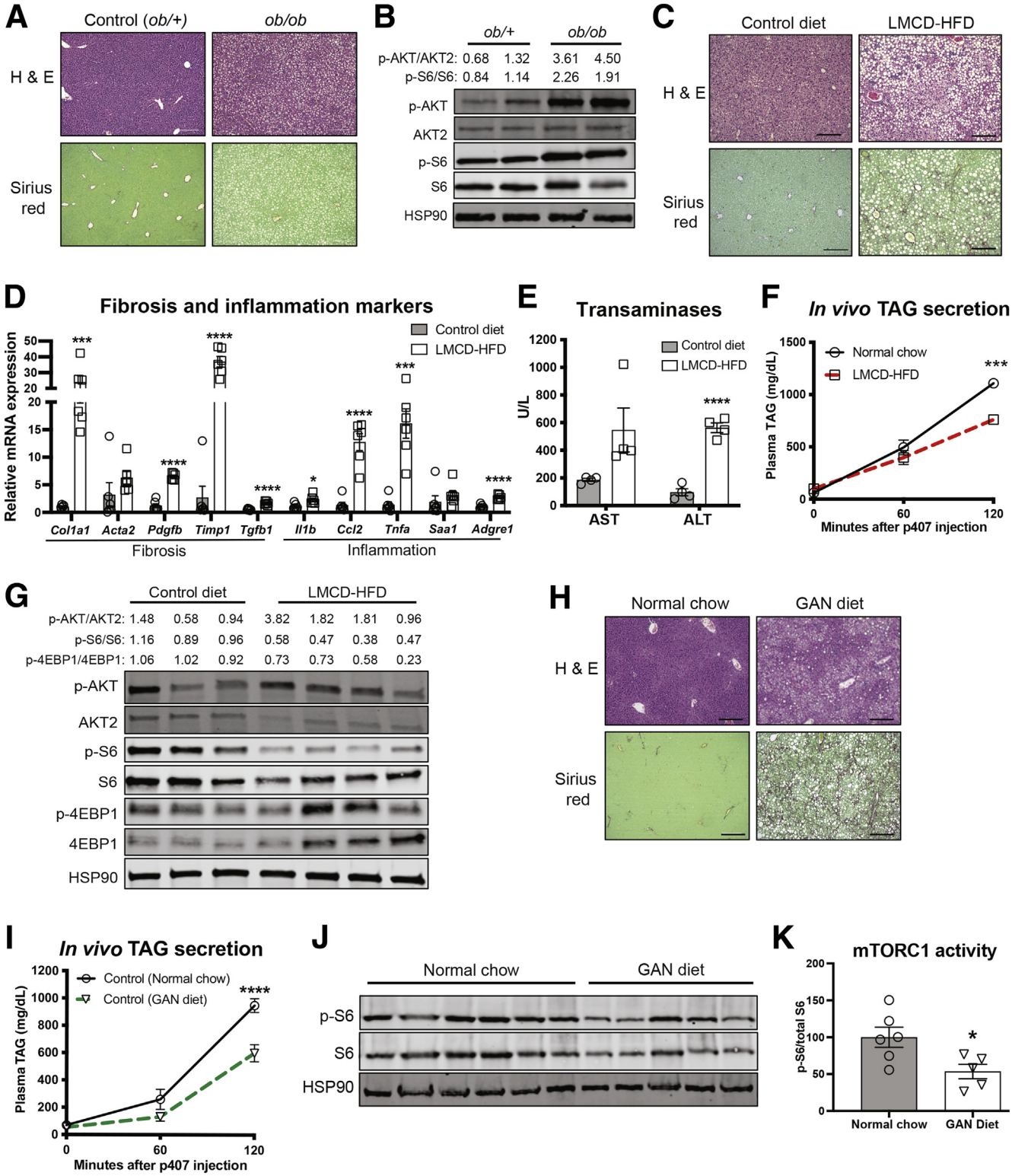

in our NASH-fed model (Figure 2*I*), in agreement with previous observations in L-TSC-KO mice fed a chow diet.[34] We also observed a parallel suppression of key hepatic lipogenic genes (*Srebp1c, Fasn,* and *Acaca*) under conditions of constitutive liver mTORC1 activity (Figure 2*J*). These changes in hepatic lipid metabolism in L-TSC-KO mice did not correlate with any alterations in body weight of the mice (Figure 2*K*), nor were there differences in glucose and insulin sensitivity and circulating fasting TAG (Figure 3*A*–*E*). Additionally, constitutive mTORC1 activity is known to block prolonged fasting-induced β-oxidation.[24] However, we did not find differences in fatty acid oxidation-associated genes (*Mcad, Ppara,* and *Cpt1a*) (Figure 3*F*) or circulating ketones (Figure 3*G*) between 6-hour-fasted LMCD-HFD-fed L-TSC-KO mice and control mice. Additionally, we did not detect an increase in apolipoprotein gene expression in L-TSC-KO mice, suggesting VLDL-TAG secretion is enhanced independent of changes in apolipoprotein expression (Figure 3*H*). Based on the known role of mTORC1 in regulating autophagy, we measured gene expression of *Lc3b* and *p62* and did not observe a difference between control and TSC-deficient livers (Figure 3*I*). This finding was consistent with similar protein levels of p62 in both cohorts of mice (Figure 3*J*). Collectively, these data suggest *in vivo* mTORC1 activation protects against diet-induced NASH through both enhancement of TAG secretion and suppression of DNL, independent of changes in body weight, insulin sensitivity, AKT signaling, or fatty acid oxidation.

Next, we tested whether acute mTORC1 activation is sufficient to reverse fibrosis and inflammation in livers with pre-established NASH. Here, we challenged $Tsc1^{loxp/loxp}$ to the LMCD-HFD for 4 weeks prior to injection of AAV8-TBG-Cre (L-TSC-KO) or -GFP (Control). Following AAV injection, mice continued LMCD-HFD feeding for an additional 4 weeks (Figure 4*A*). Functional activation of mTORC1 in L-TSC-KO mice was confirmed by increased phosphorylation of S6 and loss of TSC1 protein (Figure 4*B*). Activation of mTORC1 was followed by a decrease in fibrotic (*Col1a1, Acta2, Pdgfb,* and *Tgfb1*) and inflammatory (*Tnfa* and *Adgre1*) gene markers (Figure 4*C*) and decreased plasma ALT activity, with no significant change in AST (Figure 4*D*). Following the establishment of NASH, acute deletion of hepatic TSC1 led to a significant improvement in liver collagen deposition as documented by Sirius red staining and fibrosis staging (Figure 4*E and F*). Consistent with the NASH prevention L-TSC-KO model, improvements of fibrosis were accompanied by a reduction in hepatic steatosis (Figure 4*E and G*). Similar to the prevention study, the improvements in fibrosis and steatosis correlated with increased TAG secretion and suppression of DNL genes (*Srebp1c* and *Fasn*) (Figure 4*H and I*). These improvements in hepatic fibrosis and TAG accumulation occurred independent of changes in body weight (Figure 4*J*). In summary, these data reveal that acute *in vivo* activation of hepatic mTORC1 lowered hepatic TAG accumulation by enhancing VLDL-TAG secretion and suppressing DNL, leading to improved hallmarks of NASH in mice.

To expand our dietary models of NASH in mice, we also employed the NASH-GAN diet to evaluate the effect of mTORC1 activity on NASH resolution. Briefly, $Tsc1^{loxp/loxp}$ were fed the NASH-GAN diet for 30 weeks, injected with AAV, and sacrificed 6 weeks following AAV administration (Figure 5*A*). Gene expression measurements confirmed successful knockout of *Tsc1* in the liver (Figure 5*B*). Similar to the results obtained in the LMCD-HFD model, mTORC1 activation did not affect body weight of mice 6 weeks after AAV injection (Figure 5*C*). Hepatic mTORC1 activation improved histological collagen deposition (Figure 5*D and E*), with similar trends at the gene expression level (Figure 5*G*). Further, steatosis was improved in L-TSC-KO livers (Figure 5*F*), which correlated with reduced lipogenic gene expression (Figure 5*H*). Altogether, these data indicate that *in vivo* activation of mTORC1 protects from the development and progression of NASH in mice.

mTORC1 Controls Total Hepatic Lipid Content Through Its Regulation of VLDL-TAG Secretion and Lipid Synthesis

To mechanistically define the anti-steatotic, anti-inflammatory, and anti-fibrotic effects resulting from hepatic *Tsc1* deletion, we first evaluated the requirement of mTORC1-regulated VLDL-TAG secretion on hepatic steatosis and inflammation in chow-fed mice. VLDL synthesis and secretion are reduced in biopsy-confirmed patients with NASH compared with patients with non-fibrotic NAFL, highlighting

Figure 1. (*See previous page*). mTORC1 activity is reduced in murine NASH models. *A*–*B*, Ten-week-old *ob/ob* mice were sacrificed following a 6-hour fast. *A*, Hematoxylin and eosin (H&E) staining, and picrored (Sirius red) staining from paraffin-embedded, formalin fixed liver sections. *B*, Immunoblot of liver lysates, p-AKT (Ser473), total AKT2, p-S6 (Ser240/244), total S6, and HSP90. *C*–*D*, Eight- to 12-week-old C57BL6/J mice were fed LMCD-HFD (L-amino acid diet with 45 kcal% fat with 0.1% methionine and no added choline) or control diet (L-amino acid diet with 10 kcal% fat with methionine and choline) for 30 days and fasted 6 hours before sacrifice. *C*, H&E staining and sirius red staining from paraffin-embedded, formalin-fixed liver sections. *D*, Gene expression of fibrosis and inflammation genes, n = 6. *E*, Plasma ALT and AST, n = 4. *F*, Triglyceride secretion determined in 4-hour fasted animals by blocking uptake via i.p. injection of poloxamer 407, n = 3 per group. *G*, Immunoblot of liver lysates, p-AKT (Ser473), total AKT2, p-S6 (Ser240/244), total S6, p-4EBP1 (Thr37/46), total 4EBP1, and HSP90. *H*–*K*, Eight- to 12-week-old C57BL6/J mice were fed GAN diet (40 kcal% fat (mostly palm oil), 20 kcal% fructose and 2% cholesterol) or normal chow diet for 30 weeks. *H*, H&E staining and pico red (Sirius red) staining from paraffin-embedded, formalin-fixed liver sections from 6-hour fasted mice. *I*, Triglyceride secretion determined in 4-hour fasted animals by blocking uptake via i.p. injection of poloxamer 407, n = 4–5. *J*, Immunoblot of liver lysates, p-S6 (Ser240/244), total S6, and HSP90 from 6-hour fasted animals. *K*, Quantification of immunoblots calculated as phosphorylated protein proportional to total protein, relative to control mice samples. $^{*}P < .05$; $^{***}P < .001$; $^{****}P < .0001$ vs control using Student *t* test, or 2-way analysis of variance for (*F and I*). Data shown as mean ± standard error of the mean.

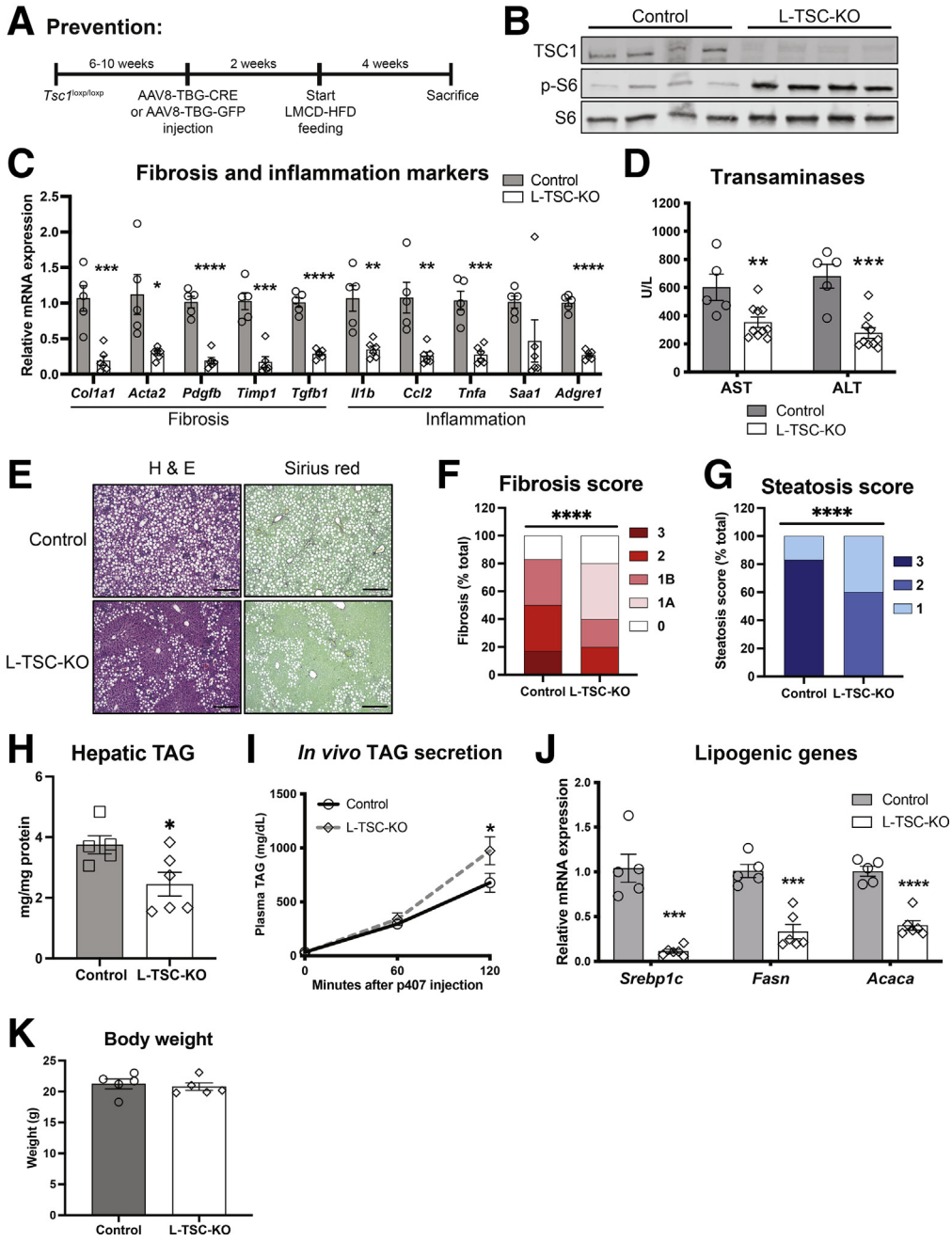

Figure 2. Acute mTORC1 activation prevents steatosis, inflammation, and fibrosis in mice on NASH diet. *A*, Experimental design schematic: 6- to 10-week-old Tsc1$^{loxp/loxp}$ animals were injected with either AAV-GFP (Control) or AAV-Cre (L-TSC-KO) 2 weeks prior to a 4-week feeding of LMCD-HFD (L-amino acid diet with 45 kcal% fat with 0.1% methionine and no added choline, Research Diets #A06071309). *B*, Representative immunoblots of liver lysates, TSC1, p-S6 (Ser240/244), and total S6. *C*, Gene expression of fibrosis and inflammation genes, n = 5–6. *D*, Plasma ALT and AST, n = 5–10. *E*, Formalin-fixed liver sections stained with hematoxylin and eosin (H&E) (general morphology) and Sirius red (collagen), representative of n = 5–6 mice. *F*, Fibrosis scoring from 0 (none) to 3 (bridging fibrosis) quantified by blinded investigator, n = 5–6. *G*, Steatosis scoring ranked from 0 (<5% steatosis) to 3 (>66% steatosis) by blinded investigator, n = 5–6. For scoring, images from 3 random fields per mouse liver section are evaluated. *H*, Hepatic TAG, n = 5–6. *I*, Triglyceride secretion determined in 4-hour fasted animals by blocking uptake via i.p. injection of poloxamer 407, n = 5 per group. *J*, Gene expression of lipogenic genes, n = 5–6. *K*, Final body weight. Data shown as mean ± standard error of the mean. *$P < .05$; **$P < .01$; ***$P < .001$; ****$P < .0001$ vs control using Student *t* test, or 2-way analysis of variance (*I*) and χ^2 test (*F and G*).

the importance of VLDL in maintaining liver lipid homeostasis.[38] VLDL production and its subsequent secretion of TAG from the liver is controlled, in part, by the biosynthesis of phosphatidylcholine (PC), the main phospholipid coating lipoproteins.[48] Numerous studies outline the importance of PC in the development of NASH, depicting that PC is

decreased in biopsy-confirmed patients with NASH compared with healthy controls.[49-51] In the liver, PC is regulated by its rate-limiting enzyme, CTP:Phosphocholine cytidylyltransferase alpha (CCTα).[52] Congenital deletion of liver CCTα protein in chow-fed mice results in hepatic steatosis due to reduced PC synthesis and impaired VLDL-TAG secretion, with no effect on liver TAG synthesis.[53] Human mutations associated with enhanced hepatic PC content are protected from NASH, further suggesting the importance of PC synthesis in the pathophysiology of NAFLD.[54,55] Recently, our lab demonstrated that mTORC1 is required for CCTα activity and VLDL-TAG secretion.[34] Consistent with this notion, levels of CCTα protein were reduced under constitutive mTORC1-inhibition, such as the deletion of Raptor protein (L-Raptor-KO) (Figure 6*A*). In contrast, constitutive activation of liver mTORC1 (L-TSC-KO) elevated levels of CCTα protein in both fasted and postprandial states (Figure 6*A*). Additionally, L-TSC-KO mice displayed an increase in CCTα protein in our diet-induced NASH prevention model (Figure 2*A*; Figure 6*B*). These changes in protein levels in L-TSC-KO were not associated with increased *Pcyt1a* expression, the gene encoding CCTα protein, suggesting mTORC1 positively regulates CCTα post-transcriptionally (Figure 6*C*).[34] The increase in CCTα protein expression led to a functional increase in PC and phosphatidylethanolamine (PE) (Figure 6*D*), which supports the enhanced TAG secretion observed in L-TSC-KO mice on NASH (Figure 2*I*; Fig. 4*H*) and L-TSC-KO mice on chow diet, as previously observed.[34] (Figure 6*E*). Overall, these key findings suggest that mTORC1 activation increases CCTα protein and hepatic PC levels leading to a functional increase in VLDL-TAG export.

To determine the epistatic relationship between CCTα and mTORC1 in the regulation of VLDL-TAG secretion under normal chow conditions, we crossed *Pcyt1a*$^{loxp/loxp}$ mice with *Tsc*$^{loxp/loxp}$ mice to generate a mouse model lacking both CCTα and TSC1 in the liver (L-CCTaTSC-double knockout [DKO]). Two weeks following AAV administration, we confirmed deletion of hepatic CCTα and TSC1 via immunoblot, which revealed loss of TSC1 and CCTα proteins and successful activation of mTORC1 through the phosphorylation of S6 (Figure 6*F*). As expected, loss of CCTα in the liver (L-CCTa-KO) completely blocked VLDL-TAG secretion in chow-fed mice (Figure 6*G*). Likewise, concomitant loss of CCTα and TSC1 reduced VLDL-TAG secretion to a similar extent to that of L-CCTa-KO (Figure 6*G*). Both L-CCTa-KO and L-CCTaTSC-DKO mice displayed increased fibrotic gene expression (*Col1a1* and *Timp1*), along with similar changes in inflammatory gene expression, apart from *Saa1*, a surprising finding for chow-fed conditions (Figure 6*H*). In parallel, L-CCTa-KO exhibited increased levels of hepatic TAG as compared with control mice, whereas L-TSC-KO mice presented with decreased hepatic TAG (Figure 6*I*). L-CCTaTSC-DKO displayed significant upregulation of hepatic TAG levels. However, this effect did not fully recapitulate the hepatic TAG levels observed in L-CCTa-KO alone, which suggests an additional role for mTORC1 in regulating total hepatic lipid content (Figure 6*I*). In support of this notion, lipogenic gene expression (*Srebp1c* and *Fasn)* in L-CCTaTSC-DKO livers were downregulated to similar levels of L-TSC-KO when compared with both control littermates and L-CCTa-KO mice that lack constitutive mTORC1 activation (Figure 6*J*). Collectively, these data reveal that mTORC1 modulates total hepatic lipid content partially through its control of VLDL-TAG secretion, but the regulation of additional lipid synthesis pathways are involved. Nevertheless, these data support the critical importance of PC and VLDL-TAG export for the onset of liver fibrosis and inflammation.

Deletion of FOXO1 in Livers With Constitutive mTORC1 Activity Restores DNL and Liver TAGs But Does Not Induce Fibrosis or Inflammation

mTORC1 activity is required for SREBP1c-driven DNL in response to insulin stimulation.[26,27] However, many groups have elucidated that activation of mTORC1 alone is not sufficient to induce lipogenesis (Figure 7*A*).[28,30,32] In support of those previous studies, we observed decreased expression of key lipogenic genes (*Srebp1c* and *Fasn)* in our L-TSC-KO NASH and chow-fed models (Figures 2*J*; 4*I*; 5*H*; and 6*J*). Additionally, suppression of lipogenic gene expression in chow-fed L-TSC-KO mice correlated with a reduction in total hepatic TAG content in L-TSC-KO mice compared with controls (Figure 6*I*). The down-regulation of SREBP1c and its targets in L-TSC-KO mice is attributed in part to a negative feedback-inhibition of mTORC2-AKT (Figure 7*A*).[28]

AKT is both required and sufficient for lipogenesis; however, the mechanisms of AKT-dependent SREBP induction remain debated.[29,56] Yecies *et al* suggest that AKT inhibition promotes *Insig2a* expression, a negative regulator of SREBPs that blocks SREBP cleavage and activation.[28] However, AKT signals through multiple pathways to regulate lipid synthesis, one of which is the phosphorylation and inhibition of the forkheadbox protein O (FOXO) transcription factors.[57] Simultaneous deletion of FOXO1 and TSC1 in AKT-deficient mouse livers completely restored lipogenesis *in vivo*, independent of increased *Insig2a* expression, suggesting that the AKT-FOXO1 signaling axis may additionally regulate DNL.[30] In our LMCD-HFD-fed models, we observed decreased levels of AKT phosphorylation following mTORC1 activation (Figure 7*B*). Moreover, we detected increased insulin-like growth factor binding protein-1 (IGFBP-1) protein levels, a direct target of FOXO, suggesting an increase in FOXO activity in L-TSC-KO liver (Figure 7*B*).[58]

To determine if upregulation of FOXO1 was driving the anti-lipogenic effects of L-TSC-KO under normal chow conditions, *Foxo1*$^{loxp/loxp}$*Tsc1*$^{loxp/loxp}$ mice were injected with AAV8-TBG-Cre (L-FOXOTSC-DKO), or -GFP (Control) 2 weeks prior to sacrifice. Deletion of hepatic *Foxo1* and *Tsc1* were confirmed by gene expression analysis (Figure 7*C*). Loss of FOXO1 under conditions of constitutive mTORC1 activation (L-FOXOTSC-DKO) induced the mRNA expression of *Srebp1c,* despite significantly high levels of *Insig2a* expression (Figure 7*D*). The changes in lipogenic gene program correlated with a trend in increase in total liver lipid content (Figure 7*E*) and *de novo* palmitate synthesis

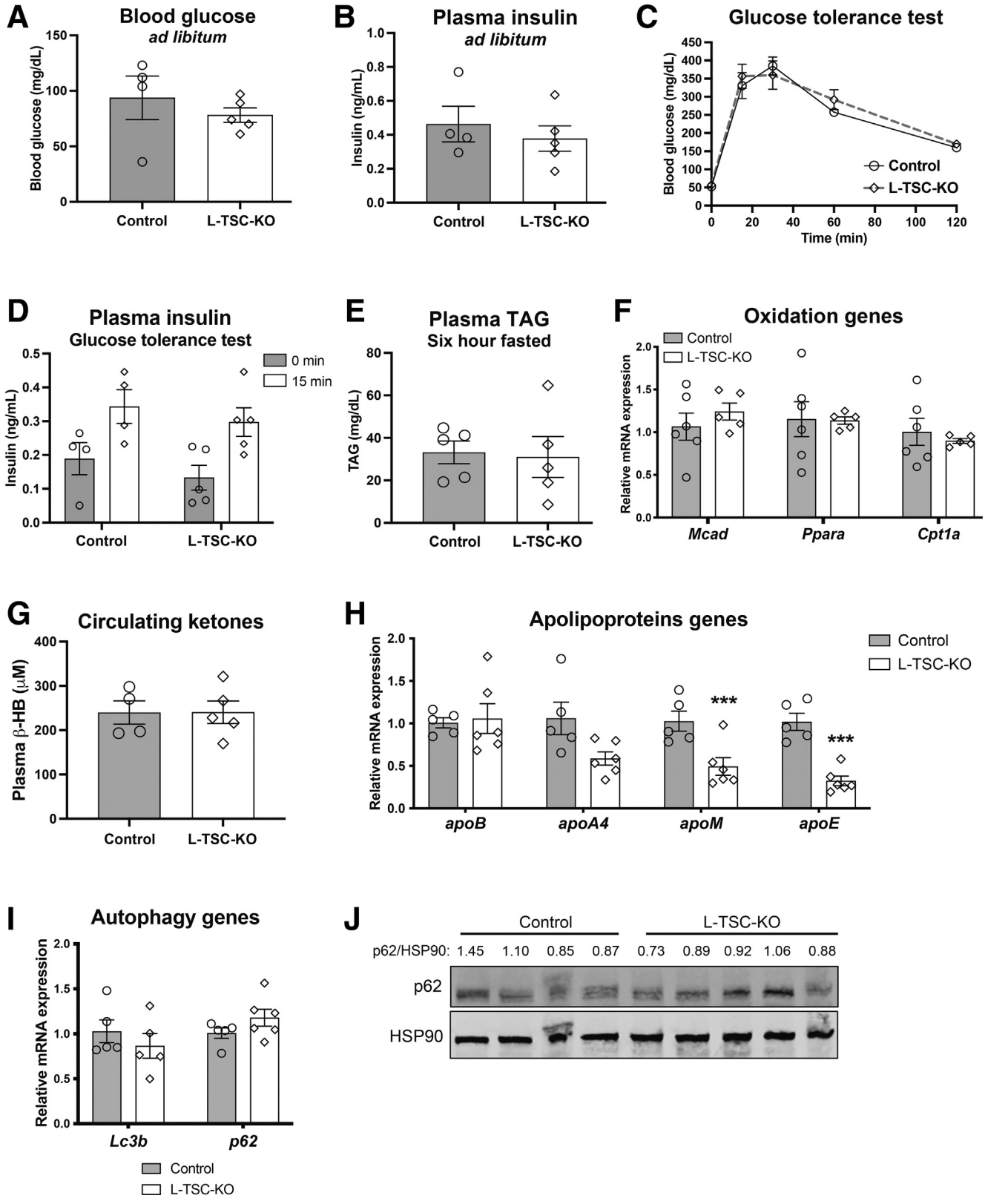

Figure 3. mTORC1 activation does not affect glucose and insulin sensitivity, fatty acid oxidation, and autophagy. *A–E*, Six- to 10-week-old $Tsc1^{loxp/loxp}$ animals were injected with either AAV-GFP (Control) or AAV-Cre (L-TSC-KO) 2 weeks prior to a 4-week feeding of LMCD-HFD. *A*, Blood glucose measured ad libitum. *B*, Plasma insulin measured ad libitum. *C*, Intraperitoneal glucose tolerance test (2 g/kg) on overnight fasted mice, n = 4–5. *D*, Insulin levels before and after 15 minutes following glucose injection. *E*, Circulating TAG in 6-hour fasted mice. *F*, Gene expression of fatty acid oxidation-related genes. *G*, Circulating β-hydroxybutyrate in 6-hour fasted mice. *H*, Gene expression of apolipoprotein genes. *I*, Gene expression of autophagy-related genes. *J*, Immunoblot of p62 from liver lysates. Quantification normalized to loading control (HSP90) and presented as relative to control (lanes 1-4). ***$P < .001$ vs control using Student *t* test. Data shown as mean ± standard error of the mean.

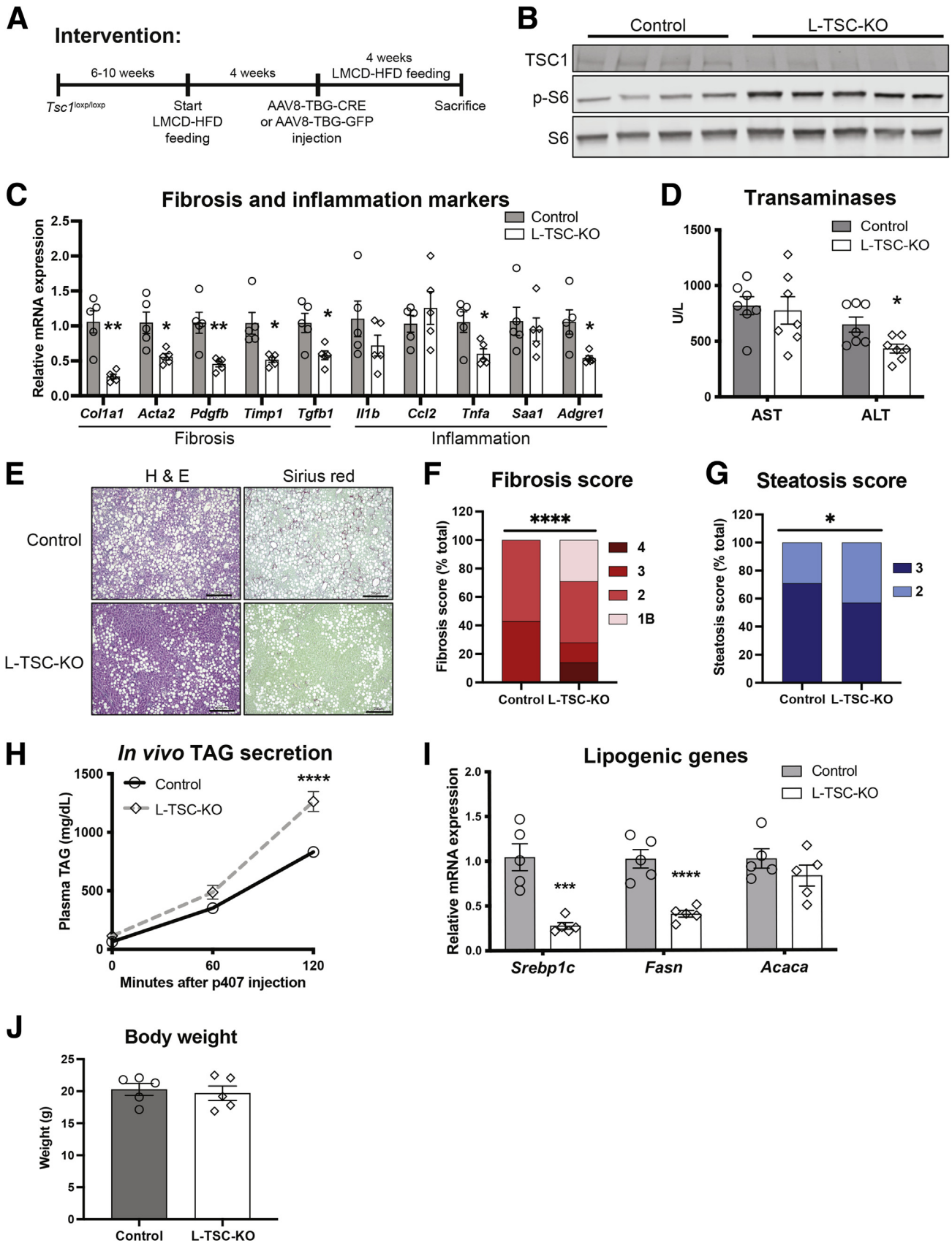
A
Intervention:
6-10 weeks
4 weeks
4 weeks
LMCD-HFD feeding
Tsc1loxp/loxp
Start
LMCD-HFD
feeding
AAV8-TBG-CRE
or AAV8-TBG-GFP
injection
Sacrifice
B
Control
L-TSC-KO
TSC1
p-S6
S6
C
Fibrosis and inflammation markers
Control
L-TSC-KO
Relative mRNA expression
Col1a1
Acta2
Pdgfb
Timp1
Tgfb1
Il1b
Ccl2
Tnfa
Saa1
Adgre1
Fibrosis
Inflammation
D
Transaminases
Control
L-TSC-KO
U/L
AST
ALT
E
H & E
Sirius red
Control
L-TSC-KO
F
Fibrosis score
Fibrosis score (% total)
4
3
2
1B
Control L-TSC-KO
G
Steatosis score
Steatosis score (% total)
3
2
Control L-TSC-KO
H
In vivo TAG secretion
Control
L-TSC-KO
Plasma TAG (mg/dL)
Minutes after p407 injection
I
Lipogenic genes
Control
L-TSC-KO
Relative mRNA expression
Srebp1c
Fasn
Acaca
J
Body weight
Weight (g)
Control
L-TSC-KO

(Figure 7*F*) in L-FOXOTSC-DKO mice. Furthermore, we observed an induction of *Gck* (Figure 7*D*), the gene encoding glucokinase, the primary hexokinase and glucose sensor in the liver that is repressed by FOXO proteins and stimulated by SREBP1c.[59,60] The restoration of lipogenic gene expression correlated with increased hepatic TAG content (Figure 7*G*). However, the increase in lipogenic gene expression and hepatic TAG content following inhibition of FOXO1 alone was not sufficient to induce fibrosis and inflammation (Figure 7*H*). These data support a hypothesis that DNL significantly contributes to hepatic TAG accumulation in NAFLD but that defects in PC biosynthesis and VLDL-TAG export are also required to induce hepatic fibrosis and inflammation.

Exogenous SREBP1c Expression Rescues DNL in Mice With Constitutive Liver mTORC1 Activity

To assess the direct contribution of DNL in our L-TSC-KO models without affecting additional FOXO1-dependent mechanisms, we injected chow-fed mice with a liver-specific AAV containing the nuclear form of SREBP1c (AAV8-TBG-nSREBP1c). SREBPs are membrane-bound transcription factors that are activated via cleavage by SREBP cleavage activating protein, leading to its subsequent translocation to the nucleus.[61-63] Notably, expression of AAV8-TBG-nSREBP1c significantly increased total liver lipid and *de novo* lipogenesis in mice challenged to a lipogenic diet (70% kcal carbohydrate, 10% kcal fat) (Figure 8*A and B*). Next, we co-administered the AAV8-TBG-nSREBP1c into $Tsc1^{loxp/loxp}$ mice in combination with either AAV-GFP (+nSREBP1c) or AAV-Cre (L-TSC-KO + nSREBP1c). Exogenous nSREBP1c successfully promoted expression of key lipogenic genes, *Srebp1c, Fasn,* and *Acaca,* to supraphysiological levels in control and L-TSC-KO livers (Figure 8*C*). Analogously, nSREBP1c overexpression led to an increase in hepatic TAG content in both +nSREBP1c and L-TSC-KO + nSREBP1c cohorts (Figure 8*D*). Consistent with our L-FOXOTSC-DKO model, re-establishment of the DNL program in TSC-deficient mice did not induce fibrosis and inflammation gene markers (Figure 8*E*). Lastly, we observed no additive effects of nSREBP1c on TAG secretion in L-TSC-KO mice (Figure 8*F*), indicating mTORC1 activation controls TAG secretion via a parallel pathway. Therefore, consistent with FOXO1 ablation, nSREBP1c expression alone restored the lipogenic gene profile and total hepatic TAG content without any indication of increased hepatic fibrosis or inflammation.

Inhibition of VLDL-TAG Secretion Promotes Fibrosis in NASH-fed Mice Under Constitutive mTORC1 Activation

Based on our finding that inhibition of CCTa promoted fibrosis and inflammation in chow-fed mice and restoring DNL did not affect fibrotic gene expression, we hypothesized that DNL significantly contributes to hepatic TAG accumulation in NAFLD but that defects in PC biosynthesis and VLDL-TAG export are critical for the induction of hepatic fibrosis and inflammation in NASH. Therefore, we tested whether restoration of DNL or inhibition of VLDL-TAG secretion under constitutive mTORC1 activity would prevent the onset of fibrosis in rodents fed LMCD-HFD NASH-promoting diet. To do so, $Pcyt1a^{loxp/loxp}Tsc1^{loxp/loxp}$ and $Foxo1^{loxp/loxp}Tsc1^{loxp/loxp}$ and mice were subjected to the LMCD-HFD for 4 weeks following injection of either AAV-Cre (L-FOXOTSC-DKO or L-CCTaTSC-DKO, respectively) or GFP -(Control) (Figure 9*A*). Excision of these genes in the liver were confirmed by decreased mRNA expression (Figure 9*B*). Remarkably, we found L-CCTaTSC-DKO mice on NASH diet had increased incidence and staging of fibrosis; however, they were still somewhat protected from steatosis compared with littermate controls on NASH diet (Figure 9*C–E*). These findings correlated with decreased VLDL-TAG secretion in L-CCTaTSC-DKO (Figure 9*F*). Next, we tested the effects of inhibiting FOXO1 in mice with constitutive mTORC1 activation to restore the lipogenic gene program (L-FOXOTSC-DKO) (Figure 9*A*). Surprisingly, we found no difference in fibrosis but increased levels of steatosis in L-FOXOTSC-DKO mice compared with NASH diet-fed controls (Figure 9*G–I*). Increased steatosis was driven by a complete restoration of the DNL gene expression (*Srebp1c, Fasn, Acaca*) (Figure 9*J*) and *de novo* palmitate synthesis (Figure 9*K*). In sum, we observed that acute mTORC1 activation prevented the development of NASH in mice, and inhibition of VLDL-TAG secretion in these mice accelerates fibrosis, but restoring DNL alone does not affect fibrosis progression.

Discussion

Data presented in this manuscript indicate that mTORC1 activity is reduced in murine NASH livers and that activation

Figure 4. (*See previous page*). Acute mTORC1 activation improves steatosis, inflammation, and fibrosis in mice on NASH diet. *A*, Experimental design schematic: 6- to 10-week-old $Tsc1^{loxp/loxp}$ animals were fed LMCD-HFD (L-amino acid diet with 45 kcal% fat with 0.1% methionine and no added choline, Research Diets #A06071309) for 4 weeks, then injected with either AAV-GFP (Control) or AAV-Cre (L-TSC-KO) and continued diet regimen for 4 more weeks. *B*, Representative immunoblots of liver lysates, TSC1, p-S6 (Ser240/244), and total S6. *C*, Gene expression of fibrosis and inflammation genes, n = 5 per group. *D*, Plasma ALT and AST, n = 6–7. *E*, Formalin-fixed liver sections stained with hematoxylin and eosin (H&E) (general morphology) and Sirius red (collagen), representative of n = 5–6 mice. *F*, Fibrosis scoring from 0 (none) to 3 (bridging fibrosis) quantified by blinded investigator, n = 5–6. *G*, Steatosis scoring ranked from 0 (<5% steatosis) to 3 (>66% steatosis) by blinded investigator, n = 5–6. For scoring, images from 3 random fields per mouse liver section are evaluated. *H*, Triglyceride secretion determined in 4-hour fasted animals by blocking uptake via i.p. injection of poloxamer 407, n = 5 per group. *I*, Gene expression of lipogenic genes, n = 5. *J*, Final body weight. Data shown as mean ± standard error of the mean. *$P < .05$; **$P < .01$; ***$P < .001$; ****$P < .0001$ vs control using Student *t* test, except 2-way analysis of variance (*H*), and χ^2 test (*F and G*).

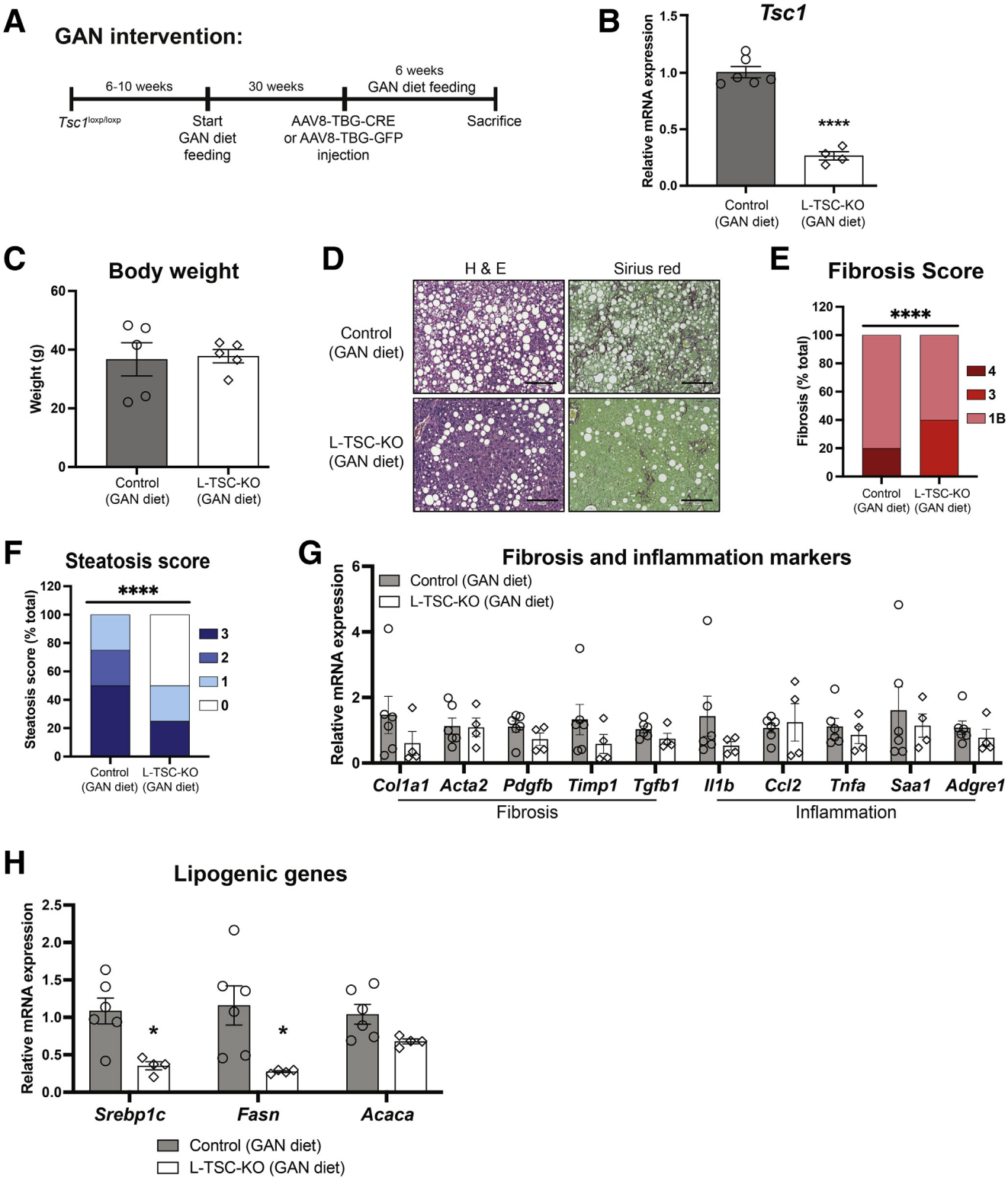

Figure 5. Acute mTORC1 activation reverses steatosis, inflammation, and fibrosis in GAN diet-fed mice. *A*, GAN diet intervention schematic: 6- to 10-week-old Tsc1$^{loxp/loxp}$ animals were fed a GAN diet (40 kcal% fat [mostly palm oil], 20 kcal% fructose, and 2% cholesterol, Research Diets #D09100310) for 30 weeks prior to AAV-GFP (Control) or AAV-Cre (L-TSC-KO) injection. Animals continued GAN diet feeding for 6 weeks after AAV injection. *B*, Tsc1 gene expression. *C*, Final body weight. *D*, Formalin-fixed liver sections stained with hematoxylin and eosin (H&E) (general morphology) and Sirius red (collagen), representative of n = 5–6 mice. *E*, Fibrosis scoring from 0 (none) to 3 (bridging fibrosis) quantified by blinded investigator, n = 4–5. *F*, Steatosis scoring ranked from 0 (<5% steatosis) to 3 (>66% steatosis) by blinded investigator, n = 4–5. For scoring, images from 3 random fields per mouse liver section are evaluated. *G*, Gene expression of inflammation and fibrosis genes. *H*, Gene expression of lipogenic genes. *$P < .05$; ****$P < .0001$ vs control using student *t* test (*B, C, G, H*) and χ^2 test (*E, F*). Data shown as mean ± standard error of the mean.

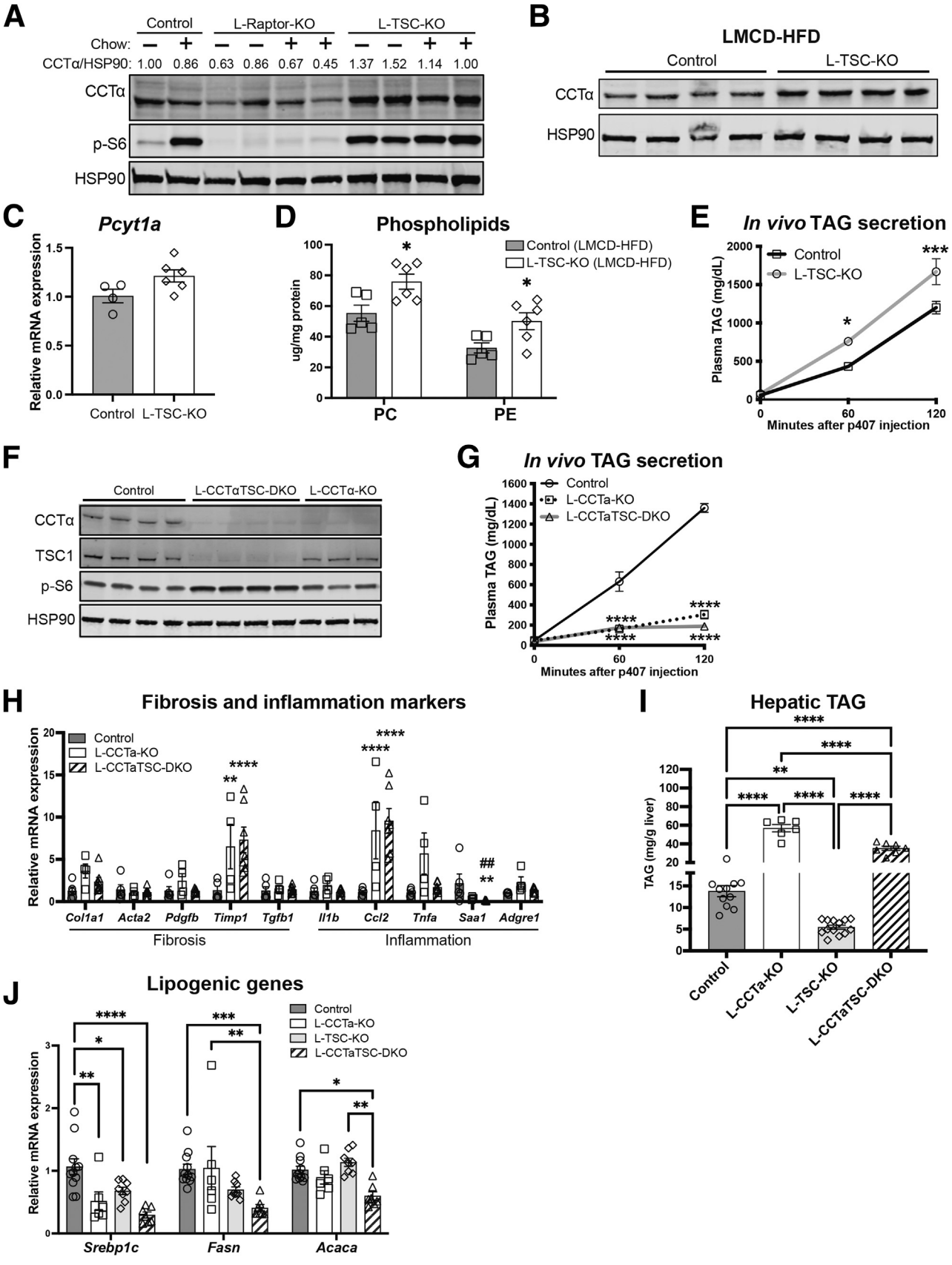
A
Control
L-Raptor-KO
L-TSC-KO
Chow: – + – + + – – + +
CCTα/HSP90: 1.00 0.86 0.63 0.86 0.67 0.45 1.37 1.52 1.14 1.00
CCTα
p-S6
HSP90
B
LMCD-HFD
Control
L-TSC-KO
CCTα
HSP90
C
Pcyt1a
Relative mRNA expression
Control L-TSC-KO
D
Phospholipids
Control (LMCD-HFD)
L-TSC-KO (LMCD-HFD)
ug/mg protein
PC
PE
E
In vivo TAG secretion
Control
L-TSC-KO
Plasma TAG (mg/dL)
Minutes after p407 injection
F
Control
L-CCTαTSC-DKO
L-CCTα-KO
CCTα
TSC1
p-S6
HSP90
G
In vivo TAG secretion
Control
L-CCTa-KO
L-CCTaTSC-DKO
Plasma TAG (mg/dL)
Minutes after p407 injection
H
Fibrosis and inflammation markers
Control
L-CCTa-KO
L-CCTaTSC-DKO
Relative mRNA expression
Col1a1 Acta2 Pdgfb Timp1 Tgfb1 Il1b Ccl2 Tnfa Saa1 Adgre1
Fibrosis
Inflammation
I
Hepatic TAG
TAG (mg/g liver)
Control
L-CCTa-KO
L-TSC-KO
L-CCTaTSC-DKO
J
Lipogenic genes
Control
L-CCTa-KO
L-TSC-KO
L-CCTaTSC-DKO
Relative mRNA expression
Srebp1c Fasn Acaca

of hepatic mTORC1 protects against and reverses NASH in mice through dual promotion of VLDL-TAG secretion and suppression of DNL. This key finding is in agreement with previous studies that observed increased AKT and mTORC1 activation in models of *ob/ob* (Figure 1*A*) and diet-induced obesity, in which enhanced DNL is a key feature of patients with early-stage NAFL.[13-15,35,39,40] These data are consistent with studies that observed enhanced liver damage and cell death upon chronic mTORC1 inhibition in mice and align with published studies that demonstrate mTORC1 activity is reduced in fibrotic regions of the liver in mice with NASH.[36,37,64] Taken together, we postulate that mTORC1 activity has a differential role in the initiation and progression of NAFLD such that its activity is enhanced under insulin-resistant, steatotic conditions, but reduced as NAFLD progresses with increases in fibrosis and inflammation. In this study, we provide new evidence that mTORC1 activity is reduced in 2 models of murine NASH and that activation of mTORC1 under these conditions may be hepatoprotective, but TAG export may be a critical regulator of the onset and progression of fibrosis.

Mechanistically, we identify 2 key pathways responsible for the protection from NASH by mTORC1. First, we demonstrate that constitutive mTORC1 activation suppresses lipogenic gene expression. As previously described, enhanced DNL is a key feature of NAFLD, making the lipogenic pathway a desirable target for the treatment of NAFLD as it protects from steatosis and thus the development of fibrosis and inflammation. Central to this is the mTORC1 signaling pathway and the subsequent activation of several downstream factors required for induction of SREBP-mediated lipogenesis.[65,66] However, mTORC1 activity alone is not sufficient for the induction of DNL, as reported by several groups.[28,30,32] Accordingly, models recapitulating constitutive mTORC1 activation observed suppression of hepatic DNL and lipogenic gene expression.[28,31,32] This phenomenon is attributed to a negative feedback inhibition of the mTORC2-AKT axis (Figure 7*A*).[28,67,68] mTORC2 phosphorylates and activates AKT at Ser473.[69] Along these lines, we detected decreased levels of AKT activity (Figure 7*B*), which we attribute to a mTORC1-mediated negative feedback regulation loop. These observations are consistent with impaired AKT activation in congenital models of TSC-deficiency, reversed by short-term treatment with mTORC1 inhibitor, rapamycin.[31] As such, AKT is both required and sufficient for the induction of lipogenesis.[29,56] However, the mechanisms of AKT-dependent lipogenesis are still debated.

Studies by the Manning group show that AKT inhibits *Insig2a* in primary hepatocytes, the gene encoding INSIG2, an inhibitory protein of SREBP, independent of changes to mTORC1 activity.[28] However, work from our laboratory suggests that inhibition of FOXO1 in AKT-deficient livers is sufficient to restore SREBP activity and lipogenesis *in vivo*, independent of changes in INSIG2.[30] Moreover, deletion of FOXO1,3,4 in murine livers induces glucokinase and SREBP expression, which, in turn, stimulates DNL.[57,70] Therefore, we postulate that inhibition of FOXO1 is required for the AKT-dependent regulation of DNL induction, as we detected a similar restoration of *Srebp1c* and *Gck* following the deletion of FOXO1 in L-TSC-KO livers. In our chow-fed L-FOXOTSC-DKO model, hepatic *Srebp1c* expression is rescued despite an induction of *Insig2a*. Nonetheless, we observed a similar impairment of AKT activation and DNL induction in L-TSC-KO mice under both chow and NASH-fed conditions. Decreased AKT activity correlated with a suppression of lipogenic gene panel and a decrease of hepatic TAG in L-TSC-KO mice. Interestingly, *in vivo* experiments that restored lipogenic gene expression and hepatic TAG content were not sufficient to induce inflammation nor drive fibrosis. Altogether, we show that mTORC1 has a biphasic role throughout NAFLD progression. In early stages of NAFLD, mTORC1 activity is elevated, correlating with increase in lipid accumulation. Thus, we predict that inhibition of mTORC1 activity in early NAFL will be beneficial in the protection against the enhanced DNL program, whereas inhibition of mTORC1 activity in progressed NASH may be undesirable.

The molecular pathways involved in NAFLD pathogenesis are heavily debated. Our data support previous studies that indicate TAG export and clearance from the liver are crucial regulators of NASH initiation and progression.

Figure 6. (*See previous page*). mTORC1 controls total hepatic lipid content through its regulation of VLDL-TAG secretion and lipid synthesis. *A*, Eight- to 10-week-old Rptor$^{loxp/loxp}$ and Tsc1$^{loxp/loxp}$ animals were injected with either AAV-GFP (Control) or AAV-Cre (L-Raptor-KO or L-TSC-KO) 2 weeks prior to sacrifice. Representative immunoblots of liver lysates from 16-hour fasted mice (Chow: −) followed by a 4-hour refeed (Chow: +). CCTα, p-S6 (Ser240/244), HSP90. CCTα protein quantification normalized to loading control (HSP90) and presented as relative to control fasted condition (lane 1). *B*, (Figure 2*A*) Six- to 10-week-old Tsc1$^{loxp/loxp}$ animals injected with either AAV-GFP (Control) or AAV-Cre (L-TSC-KO) 2 weeks prior to a 4-week feeding of LMCD-HFD. *A*, Immunoblot of livers from NASH prevention mice. *C*, Gene expression of Pcyt1a from chow-fed mice described in (*A*) n = 4–6. *D*, PC and phosphatidylethanolamine (PE) measured by high performance liquid chromatography from NASH mice described in (*B*). *E–H*, Eight- to 10-week-old Tsc1$^{loxp/loxp}$ animals were injected with either AAV-GFP (Control) or AAV-Cre (L-TSC-KO) and Pcyt1a$^{loxp/loxp}$Tsc1$^{loxp/loxp}$ and Pcyt1a$^{loxp/loxp}$ animals were injected with either AAV-GFP (Control) or AAV-Cre (L-CCTαTSC-DKO or L-CCTα-KO, respectively) 2 weeks prior to sacrifice. All animals remained on normal chow diet regimen. *E*, Triglyceride secretion determined in 4-hour fasted animals by blocking uptake via i.p. injection of poloxamer-407, n = 3–5. *F*, Representative immunoblots of liver lysates from 6-hour-fasted mice, n = 3–4. CCTα, TSC1, p-S6 (Ser240/244), HSP90. *G*, Triglyceride secretion, n = 7; L-CCTα-KO, n = 3. *H*, Gene expression of inflammation and fibrosis genes, n = 7 per group; L-CCTα-KO, n = 4. *I*, Hepatic triglycerides of 6-hour fasted mice, n = 6–13. *J*, Gene expression of lipogenic genes, n = 6–11. Data shown as mean ± standard error of the mean. *$P < .05$; **$P < .01$; ***$P < .001$; ****$P < .0001$ vs control or as indicated using Student *t* test (*C, D*), 2-way analysis of variance (*E, G, H, J*), or 1-way analysis of variance (*I*).

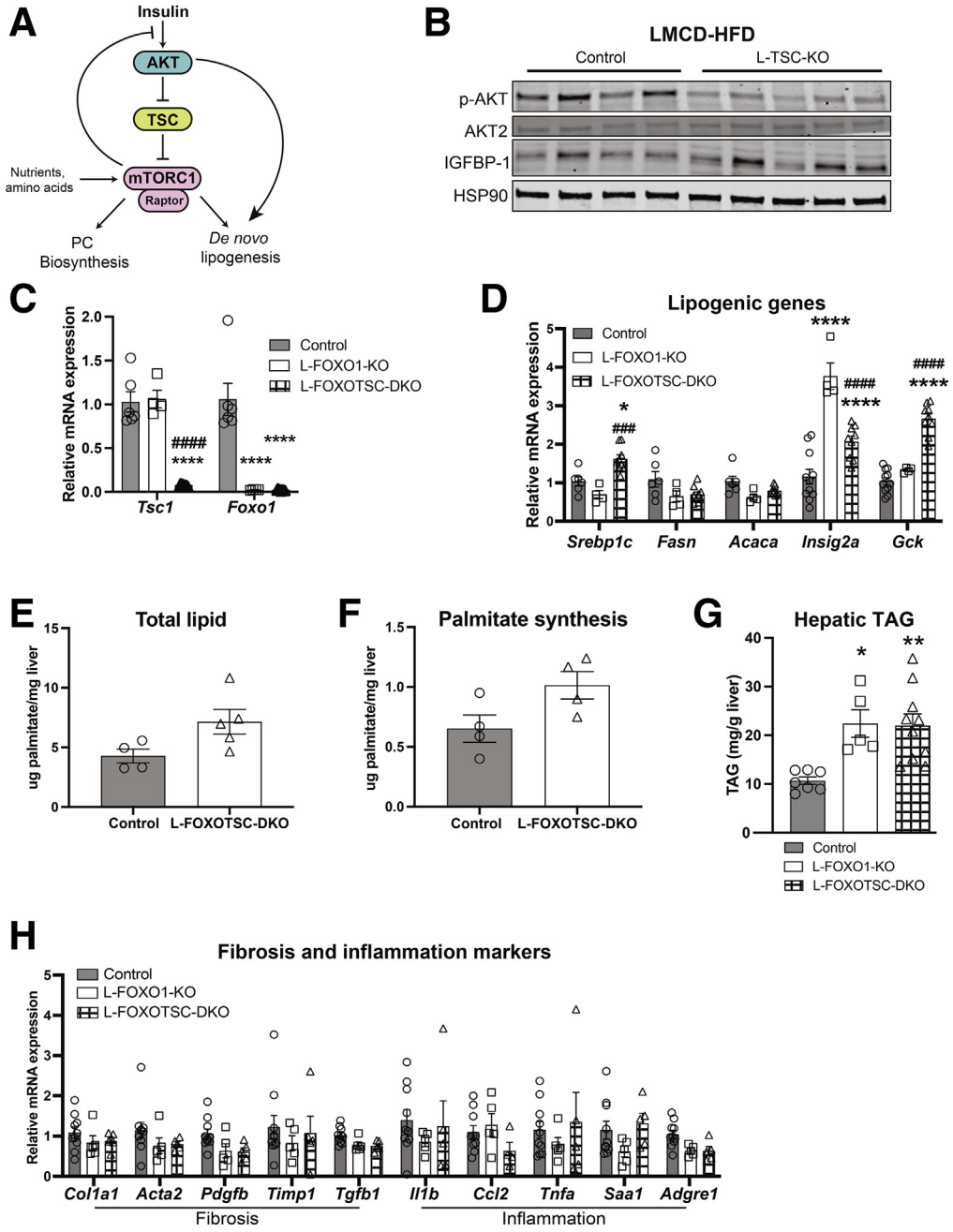

Figure 7. Deletion of FOXO1 in livers with constitutive mTORC1 activity restores DNL and liver TAGs but does not induce fibrosis or inflammation. *A*, Schematic: insulin stimulates the activation of AKT/PKB. AKT phosphorylates and inhibits the TSC complex, leading to the activation of mTORC1. mTORC1, which is recognized by its Raptor protein component, is required and sufficient for *de novo* lipogenesis and PC biosynthesis. AKT is required for induction of DNL through an mTORC1-independent pathway. However, mTORC1 negatively inhibits AKT activity, and thus activation of mTORC1 leads to a substantial decrease in AKT phosphorylation and activation. Nutrients, growth factors, amino acids, and other stimulants may activate mTORC1 independent of the insulin/AKT/TSC pathway. *B*, Immunoblot of livers of p-AKT (Ser473) from NASH prevention mice (Figure 2*A*): 6- to 10-week-old $Tsc1^{loxp/loxp}$ animals injected with either AAV-GFP (Control) or AAV-Cre (L-TSC-KO) 2 weeks prior to a 4-week feeding of LMCD-HFD. *C–H*, Eight- to 10-week-old $Foxo1^{loxp/loxp}Tsc1^{loxp/loxp}$ and $Foxo1^{loxp/loxp}$ animals were injected with either AAV-GFP (Control) or AAV-Cre (L-FOXOTSC-DKO or L-FOXO1-KO, respectively) for 2 weeks prior to sacrifice. *C*, Gene expression of Foxo1 and Tsc1, n = 4–5. *D*, Gene expression of lipogenic genes, n = 4–5. *E*, Total hepatic palmitate following 4-hour refeed. *F*, Palmitate synthesis following 4-hour refeed. *G*, Hepatic triglycerides of 6-hour fasted mice, n = 5–10. *H*, Gene expression of inflammation and fibrosis genes, n = 5–6. Data shown as mean ± SEM. **P* < .05; ***P* < .01; ****P* < .001; *****P* < .0001 vs control, ###*P* < .001; ####*P* < .0001 L-FOXOTSC-DKO vs L-FOXO1-KO using Student *t* test (*E, F*), 1-way analysis of variance (*G*), or 2-way analysis of variance (*C, D, H*).

Clinical studies in humans found VLDL-TAG synthesis and secretion are reduced in patients with fibrotic NASH livers compared with patients with fatty liver, implicating the role of VLDL in the progression to fibrosis.[38] PC is the main phospholipid coating lipoproteins and is a critical determinant of VLDL-TAG export from the liver.[48,71] Patients that received total parenteral nutrition excluding choline developed steatosis, which was reversed with choline supplementation, indicating the importance of choline and PC in maintaining hepatic lipid homeostasis.[72] Wild-type mice challenged to a high-fat diet (HFD) develop steatosis; however, mice that lack hepatic CCTα develop NASH within 1 week of HFD feeding, attributed to the decrease in hepatic PC ratios and blunting of TAG export.[50] Along these lines, several groups have mapped the lipid profiles of NAFLD in clinical studies and found that hepatic PC content is negatively correlated with increased severity of NAFLD.[49,51,54,72-76] Early rodent studies measuring PC and another major phospholipid, phosphatidylethanolamine (PE), identified a correlation between liver damage and decreased PC to PE ratio, implicating PC and PE in the progression of NAFLD.[49] In this present study, we detect increased PC and PE in L-TSC-KO mice that are protected from NASH.

In human studies, carriers of the I148M loss-of-function mutation in patatin-like phospholipase domain–containing protein 3 (PNPLA3) have an increased risk of developing NAFLD, which correlates with decreased PC synthesis and increased hepatic TAG content.[75,77] Furthermore, variants that are protective against NASH have increased hepatic PC content. First, carriers of the protein-truncating variant (rs72613567T>TA) in the hepatic lipid droplet protein hydroxysteroid 17-β dehydrogenase 13 protein, are enriched with liver PC and are protected from fibrosis.[54,55] Second, a coding variant (rs2642438G>A) in mitochondrial amidoxime reducing component 1 (MARC1) gene associates with decreased severity of NAFLD, correlating with increased plasma TAG and hepatic PC content.[73,74] Additionally, an E167K variant in the TM6SF2 gene correlates with abnormalities in ApoB trafficking and VLDL secretion, leading to an increased risk of NAFLD and progression to NASH.[76,78,79] Lastly, mutations in MTTP (rs2306986), a protein required for VLDL assembly, was associated with higher susceptibility of NAFLD.[80,81] Collectively, these studies support the hypothesis that defects in hepatic PC content and VLDL-TAG secretion significantly contribute to NASH progression. In our study, we demonstrate that suppression of VLDL-TAG secretion, and not solely the induction of the lipogenic programming, was sufficient to induce markers of fibrosis and inflammation in chow-fed and NASH diet conditions. Taken together, hepatic TAG export may play a key role in the induction of inflammation and fibrosis. Future lipidomic studies will profile both hepatic and circulating lipids to define how hepatic mTORC1 controls specific species and classes of TAGs and phospholipids.

Although our findings shed light on the role of mTORC1 in NASH and we provide evidence that VLDL-TAG secretion is critical for the promotion of fibrosis, the primary cause of death of patients with NASH is cardiovascular disease[82]; therefore, the cardiovascular impacts of mTORC1 activation in mice should be further evaluated before determining the therapeutic efficacy. Furthermore, in this study, we utilize mouse models with constitutive liver mTORC1 activation through deletion of TSC1 in an acute and inducible setting. Although long-term deletion of TSC is associated with tumorigenesis,[83] and directly inhibiting the TSC complex in human patients is not therapeutically attractive, our study provides several key mechanistic insights into the role of mTORC1 signaling responsible for driving the initiation and progression of NASH in mice. Moreover, our data are consistent with the hypothesis that insulin signaling via AKT is intact throughout the NAFL to NASH transition, consistent with elevated hepatic lipid synthesis. In early stages of simple steatosis, mTORC1 is elevated to support lipid synthesis and export. In more advanced liver disease such as NASH, mTORC1 activity is reduced, which may lead to decreased phosphatidylcholine synthesis and VLDL-TAG export, thereby promoting inflammation and fibrosis. Future studies will aim to identify novel ways to selectively modify mTORC1 activity to mimic its downstream protective effects in NASH, potentially through its role in regulating PC biosynthesis, VLDL-TAG secretion, and suppressive effects on lipogenesis. In addition, the activity status of liver mTORC1 in human NAFL and NASH needs to be determined. In summary, this study provides novel insights for the role of liver mTORC1 signaling in the pathogenesis of NAFLD.

Methods

Animal Experiments

Rptor$^{loxp/loxp}$, *Tsc1*$^{loxp/loxp}$, *Pcyt1a*$^{loxp/loxp}$, and *Foxo1*$^{loxp/loxp}$ mice were backcrossed to the C57BL/6 background,[24,53,84] housed, and bred under specific pathogen-free conditions in facilities at the University of Pennsylvania. Twelve-week-old B6-*Lep*^{ob} homozygotes (referred to here as *ob/ob*) were purchased from Jackson Laboratories (#000632), and B6-*Lep*^{ob} heterozygotes were used as controls (*ob/+*). For acute excision of liver-specific genes, mice were injected with adeno-associated virus (Vector Core, University of Pennsylvania) containing a liver-specific TBG promoter serotype 8 (AAV8-TBG) carrying Cre recombinase, at a dosage of 1.0×10^{11} genome copies at 6 to 10 weeks of age and maintained on respective feeding regimens (Figure 2*A*; 4*A*; 5*A*; and 9*A*). (AAV8-TBG-nSREBP1c virus was a kind gift from Dr Mitchell Lazar (University of Pennsylvania). All mice were fed chow diet (LabDiet, #5010) unless specified otherwise. Mice fed the LMCD-HFD were given L-Amino Acid diet with 45 kcal% fat with 0.1% methionine and no added choline (Research Diets, #A06071309). Mice fed control diets were given L-Amino Acid diet with 10 kcal% fat with methionine and choline (Research diets, A06071314). Mice fed the GAN diet were fed rodent diet with 40 kcal% fat (mostly palm oil), 20 kcal% fructose, and 2% cholesterol (Research Diets, #D09100310). Mice fed high-carbohydrate diets were fed rodent diet with 10 kcal% fat (Sucrose Diet) (Research Diets, #D12450B). All animal diets were irradiated. Control animals consist of pools of the appropriate floxed mice for each experiment (*Rptor*$^{loxp/}$

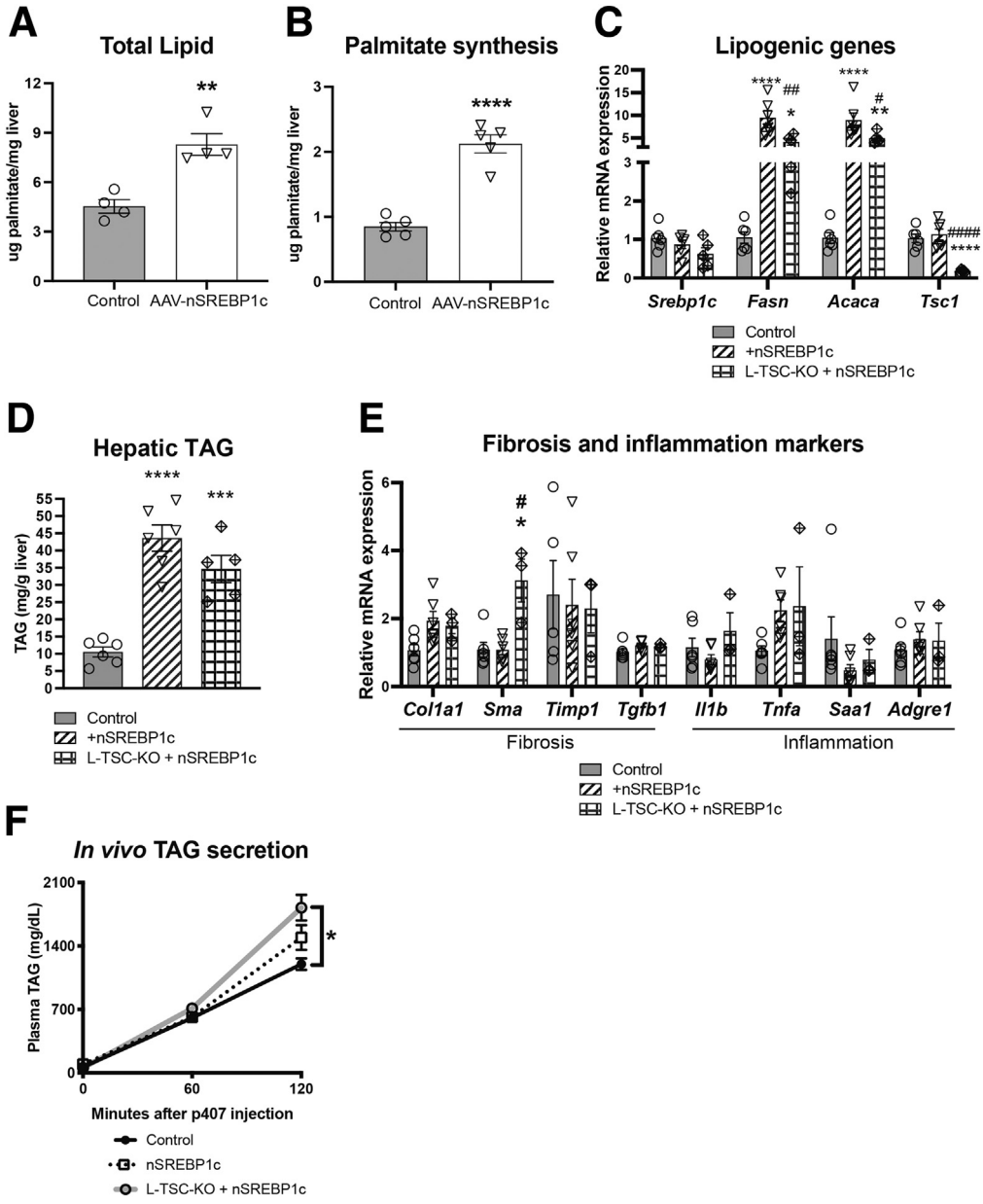

Figure 8. Exogenous SREBP1c expression rescues DNL in L-TSC-KO mice. Eight- to 10-week-old Tsc1$^{loxp/loxp}$ animals were injected with either AAV-GFP (Control), AAV-Cre (L-TSC-KO), AAV-nSREBP1c (nSREBP1c), or AAV-Cre + AAV-nSREBP1c (L-TSC-KO +nSREBP1c) for 2 weeks prior to sacrifice. *A*, Two weeks after AAV injection, mice were fed high-carbohydrate diet (Research Diets, # D12450Bi) for 3 days. Total hepatic palmitate normalized to weight liver. *B*, Palmitate synthesis following 4-hour refeed. *C*, Gene expression of lipogenic genes. *D*, Hepatic triglycerides from 6-hour fasted mice. *E*, Gene expression of inflammation and fibrosis markers. *F*, Triglyceride secretion determined in 4-hour fasted animals by blocking uptake via i.p. injection of poloxamer 407, n = 4 per group. $^{*}P < .05$; $^{**}P < .01$; $^{***}P < .001$; $^{****}P < .0001$ vs. control; ###$P < .001$ vs +nSREBP1c using Student *t* test (*A, B*), 1-way analysis of variance (*C, D, E*), or 2-way analysis of variance (*F*). Data shown as mean ± standard error of the mean.

^{loxp}, *Tsc1*$^{loxp/loxp}$, *Pcyt1a*$^{loxp/loxp}$, *Pcyt1a*$^{loxp/loxp}$*Tsc1*$^{loxp/loxp}$, *Foxo1*$^{loxp/loxp}$, and *Foxo1*$^{loxp/loxp}$*Tsc1*$^{loxp/loxp}$) that were injected with AAV8-TBG-GFP. Mice that were co-injected with AAV8-TBG-nSREBP1c and AAV8-TBG-Cre received 1.0 × 10^{11} genome copies of respective virus for a total of 2.0 x 10^{11} genome copies in a singular injection. Consistently, control mice were injected with 2.0 x 10^{11} genome copies of AAV8-TBG-GFP. All experiments were performed in male mice.

In Vivo Triglyceride Secretion

Triglyceride secretion was measured *in vivo* by intraperitoneal (i.p.) injection of 1 mg/kg poloxamer-407 in sterile-saline following a 4-hour fast, as previously described.[47] Accumulation of triglycerides in the serum were measured with Infinity Triglycerides (Thermo Scientific, TR22421).

Metabolic Measurements

For experiments involving fasting, mice were deprived of food overnight for 16 hours. For refeeding experiments, mice were overnight fasted and refed normal chow for 4 hours before blood and liver samples were collected. Plasma insulin measurements (Ultra-Sensitive Rat Insulin ELISA kit, Crystal Chem, Inc) were performed on plasma collected from mice ad libitum or 6-hour fasted. Plasma AST and ALT were measured through IDEXX VetTEST Chemistry

Analyzer. For phospholipid and TAG quantifications, liver homogenate equivalent to 1 mg protein was extracted in the presence of a phosphatidyldimethylethanolamine internal standard using a modified Folch method.[85] Phoshatidylcholine, phosphatidylethanolamine, TAG, free cholesterol, and cholesterol-ester were measured by high performance

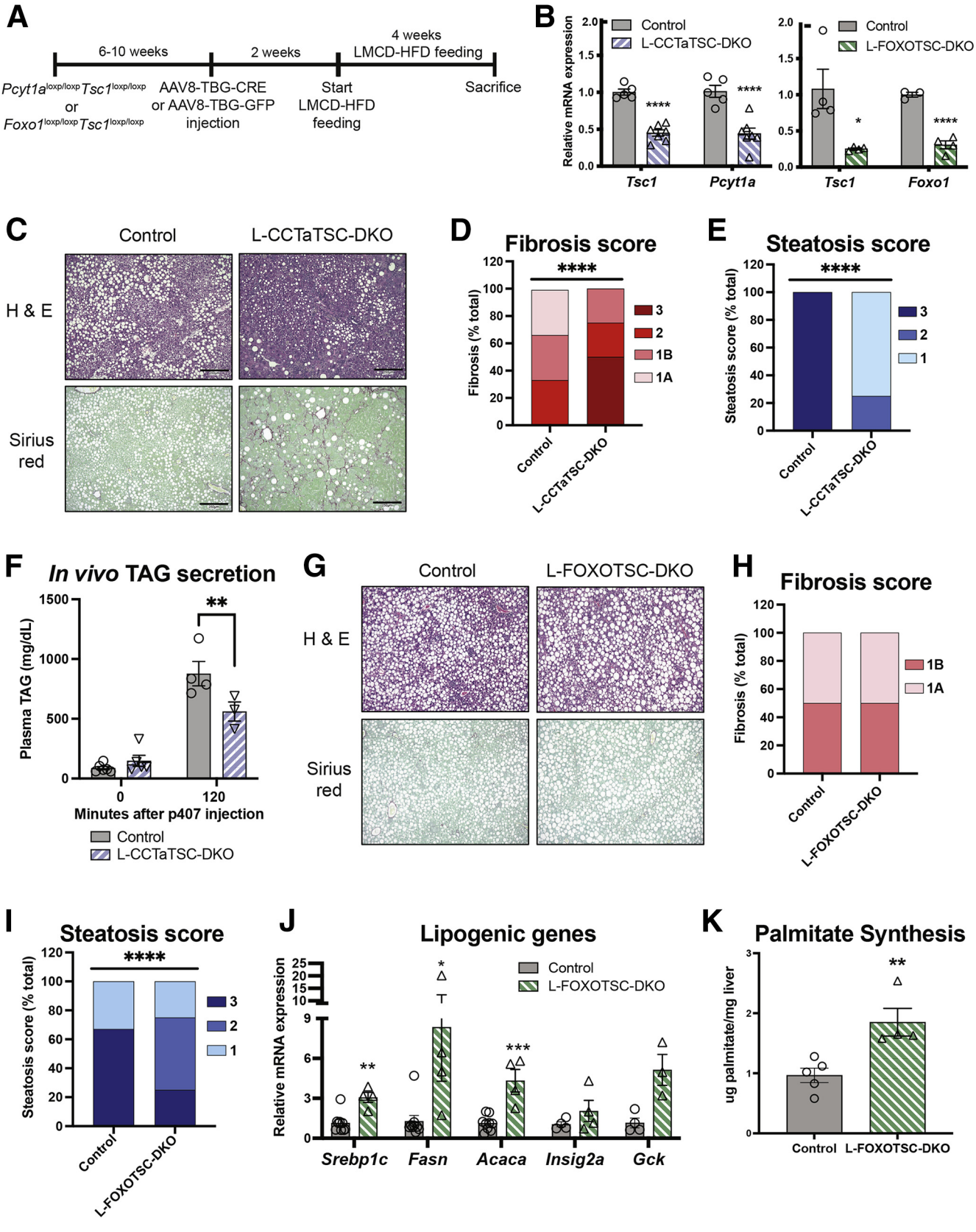

liquid chromatography, as previously described.[86,87] Hepatic TAG levels were also quantified as described before using Infinity Triglycerides (Thermo Scientific, TR22421).[88]

Glucose Tolerance Test

Overnight fasted mice were injected with 2 g/kg of glucose solution intra-peritoneally. Blood was collected and blood glucose was measured at 0, 15, 30, 60, and 120 minutes after glucose injection using OneTouch Ultra (Lifescan) glucose strips.

Immunoblots

Protein lysates were prepared from frozen livers or in a modified RIPA buffer with Phosphatase Inhibitor Cocktails 2 and 3 (Sigma-Aldrich) and cOmplete Protease Inhibitor Cocktail (Roche), as described previously.[30] Samples were separated on 4% to 15% Mini-PROTEAN TGX pre-cast gels. The following primary antibodies were used for immunoblotting: p-Akt (CST #4060), Akt2 (CST #2964), p-S6 (CST #2215), S6 (CST #2217), p-4E-BP1 (CST #236B4), 4E-BP1 (CST #9452), Tsc1 (CST #6935), CCTα (CST #6931), IGFBP1 (Santa Cruz, #sc-6000), p62 (CST #5114), HSP90 (CST #4874). Blots were developed using LI-COR Odyssey Imaging System and quantified relative to total protein controls using Image Studio Lite (LI-COR).

De Novo Lipogenesis Measurement

The amount of newly made hepatic lipid was determined as previously described.[29] Briefly, mice were fed high-carbohydrate diet (Research Diets #D12450B) for 2 days and fasted overnight. Following the overnight fast, mice were fed for 3 hours then injected i.p. with D_2O and allowed access to food for a following 3 hours. Plasma and liver samples were collected 6 hours post-feeding. Palmitate was analyzed using GC/MS, and the absolute amount of newly made palmitate was assumed equivalent to the DNL rate.

mRNA Isolation and Real-Time Polymerase Chain Reaction (PCR)

Total RNA was isolated from frozen livers using the RNeasy Plus kit (Qiagen). Complementary DNA was synthesized using Moloney murine leukemia virus reverse transcriptase, and the expression of the genes of interest was quantified by real-time PCR using the SYBR Green dye-based assay via ΔΔCT method, relative to TATA-box-binding protein.

Histology

Livers were fixed in 10% buffered formalin overnight, dehydrated in ethanol, paraffin-embedded, and sectioned. Sections were stained with hematoxylin and eosin or picro red stain 0.1% direct red 80 (#365548, Sigma) plus 0.1% fast green FCF (ab146267, Abcam). Slides were scored by a masked investigator for steatosis and stage of fibrosis. Steatosis, referred to as amount of surface area involved by steatosis as evaluated on low- to medium-power examination, as previously described,[89] on a scale of 0 (<5%), 1 (5%–33%), 2 (>33%–66%), and 3 (>66%). Fibrosis stage were evaluated as previously described,[89] on a scale of 0 (None), 1 (perisinusoidal or periportal), 1A (mild, zone 3, perisinusoidal defined as "delicate" fibrosis), 1B

(moderate, zone 3, perisinusoidal defined as "dense" fibrosis), 1C (portal/periportal with portal and/or periportal fibrosis without accompanying pericellular/perisinusoidal fibrosis), 2 (perisinusoidal and portal/periportal), 3 (bridging fibrosis), and 4 (cirrhosis).

Statistical Analysis

Statistical analysis was performed using 1-way analysis of variance when more than 2 groups were compared, 2-way analysis of variance when 2 or more conditions were analyzed followed by Sidak's multiple comparisons test (2 groups) or Tukey multiple comparisons test (>2 groups), and unpaired 2-tailed Student *t* test when 2 groups were being assayed. All data were presented as mean ± standard error of the mean. A single asterisk indicates P value $< .05$, double asterisks indicate P value $< .01$, triple asterisks indicate P value $< .001$, and four asterisks indicate P value $< .0001$ vs control.

Study Approval

The institutional animal care and use committees of the University of Pennsylvania approved all the animal studies, which adhered to the National Institutes of Health guidelines for the care and use of laboratory animals.

Figure 9. (***See previous page***). **Inhibition of VLDL-TAG secretion promotes fibrosis in NASH-fed mice under constitutive mTORC1 activation.** *A*, Experimental design schematic: 6- to 10-week-old Foxo1loxp/loxpTsc1loxp/loxp and Pcyt1a$^{loxp/loxp}$Tsc1$^{loxp/loxp}$ animals were fed LMCD-HFD (L-amino acid diet with 45 kcal% fat with 0.1% methionine and no added choline, Research Diets #A06071309) for 4 weeks, then injected with either AAV-GFP (Control) or AAV-Cre (L-FOXOTSC-DKO or L-CCTaTSC-DKO, respectively) and continued diet regimen for 4 more weeks. *B*, Gene expression of Tsc1 and Pcyt1a or Foxo1 n = 4–5. *C*, Formalin-fixed liver sections stained with hematoxylin and eosin (H&E) (general morphology) and Sirius red (collagen), representative of n = 3–5 mice. *D*, Fibrosis scoring from 0 (none) to 3 (bridging fibrosis) quantified by blinded investigator, n = 3–4. *E*, Steatosis scoring ranked from 0 (<5% steatosis) to 3 (>66% steatosis) by blinded investigator, n = 3–4. For scoring, images from 3 random fields per mouse liver section are evaluated. *F*, Triglyceride secretion determined in 4-hour fasted animals by blocking uptake via i.p. injection of poloxamer 407, n = 3–5. *G*, Formalin-fixed liver sections stained with H&E (general morphology) and Sirius red (collagen), representative of n = 4 mice. *H*, Fibrosis scoring, n = 4 mice. *I*, Steatosis scoring, n = 4 mice. *J*, Gene expression of lipogenic genes, n = 3–4. *K*, Palmitate synthesis following 4-hour refeed. Data shown as mean ± SEM. **P* < .05; ***P* < .01; ****P* < .001; *****P* < .0001 vs control using Student *t* test (*B, J, K*), except 2-way analysis of variance (*H*), and χ^2 test (*D, E, H, I*).

References

1. Younossi ZM, Koenig AB, Abdelatif D, Fazel Y, Henry L, Wymer M. Global epidemiology of nonalcoholic fatty liver disease—meta-analytic assessment of prevalence, incidence, and outcomes. Hepatology 2016;64:73–84.
2. Cohen JC, Horton JD, Hobbs HH. Human fatty liver disease: old questions and new insights. Science 2011; 332:1519–1523.
3. Chalasani N, Younossi Z, Lavine JE, Diehl AM, Brunt EM, Cusi K, Charlton M, Sanyal AJAmerican Gastroenterological Association; American Association for the Study of Liver Diseases; American College of Gastroenterology. The diagnosis and management of non-alcoholic fatty liver disease: practice guideline by the American Gastroenterological Association, American Association for the Study of Liver Diseases, and American College of Gastroenterology. Gastroenterology 2012; 142:1592–1609.
4. Ibrahim SH, Hirsova P, Gores GJ. Non-alcoholic steatohepatitis pathogenesis: sublethal hepatocyte injury as a driver of liver inflammation. Gut 2018;67:963–972.
5. Younossi Z, Stepanova M, Ong JP, Jacobson IM, Bugianesi E, Duseja A, Eguchi Y, Wong VW, Negro F, Yilmaz Y, Romero-Gomez M, George J, Ahmed A, Wong R, Younossi I, Ziayee M, Afendy A; Global Nonalcoholic Steatohepatitis Council. Nonalcoholic steatohepatitis is the fastest growing cause of hepatocellular carcinoma in liver transplant candidates. Clin Gastroenterol Hepatol 2019;17:748–755.e3.
6. Targher G, Mantovani A, Byrne CD, Wang XB, Yan HD, Sun QF, Pan KH, Zheng KI, Chen YP, Eslam M, George J, Zheng MH. Risk of severe illness from COVID-19 in patients with metabolic dysfunction-associated fatty liver disease and increased fibrosis scores. Gut 2020;69:1545–1547.
7. Promrat K, Kleiner DE, Niemeier HM, Jackvony E, Kearns M, Wands JR, Fava JL, Wing RR. Randomized controlled trial testing the effects of weight loss on nonalcoholic steatohepatitis. Hepatology 2010; 51:121–129.
8. Vilar-Gomez E, Martinez-Perez Y, Calzadilla-Bertot L, Torres-Gonzalez A, Gra-Oramas B, Gonzalez-Fabian L, Friedman SL, Diago M, Romero-Gomez M. Weight loss through lifestyle modification significantly reduces features of nonalcoholic steatohepatitis. Gastroenterology 2015;149:367–378.e5; quiz: e14–15.
9. Parker BM, Wu J, You J, Barnes DS, Yerian L, Kirwan JP, Schauer PR, Sessler DI. Reversal of fibrosis in patients with nonalcoholic steatohepatosis after gastric bypass surgery. BMC Obes 2017;4:32.
10. Younossi ZM, Ratziu V, Loomba R, Rinella M, Anstee QM, Goodman Z, Bedossa P, Geier A, Beckebaum S, Newsome PN, Sheridan D, Sheikh MY, Trotter J, Knapple W, Lawitz E, Abdelmalek MF, Kowdley Kv, Montano-Loza AJ, Boursier J, Mathurin P, Bugianesi E, Mazzella G, Olveira A, Cortez-Pinto H, Graupera I, Orr D, Gluud LL, Dufour JF, Shapiro D, Campagna J, Zaru L, MacConell L, Shringarpure R, Harrison S, Sanyal PAJ; REGENERATE Study Investigators. Obeticholic acid for the treatment of non-alcoholic steatohepatitis: interim analysis from a multicentre, randomised, placebo-controlled phase 3 trial. Lancet 2019;394:2184–2196.
11. Friedman SL, Ratziu V, Harrison SA, Abdelmalek MF, Aithal GP, Caballeria J, Francque S, Farrell G, Kowdley KV, Craxi A, Simon K, Fischer L, Melchor-Khan L, Vest J, Wiens BL, Vig P, Seyedkazemi S, Goodman Z, Wong VWS, Loomba R, Tacke F, Sanyal A, Lefebvre E. A randomized, placebo-controlled trial of cenicriviroc for treatment of nonalcoholic steatohepatitis with fibrosis. Hepatology 2018;67:1754–1767.
12. Harrison SA, Bashir MR, Guy CD, Zhou R, Moylan CA, Frias JP, Alkhouri N, Bansal MB, Baum S, Neuschwander-Tetri BA, Taub R, Moussa SE. Resmetirom (MGL-3196) for the treatment of non-alcoholic steatohepatitis: a multicentre, randomised, double-blind, placebo-controlled, phase 2 trial. Lancet 2019; 394:2012–2024.
13. Lambert JE, Ramos-Roman MA, Browning JD, Parks EJ. Increased de novo lipogenesis is a distinct characteristic of individuals with nonalcoholic fatty liver disease. Gastroenterology 2014;146:726–735.
14. Donnelly KL, Smith CI, Schwarzenberg SJ, Jessurun J, Boldt MD, Parks EJ. Sources of fatty acids stored in liver and secreted via lipoporteins in patients with NAFLD. J Clin Invest 2005;115:1343–1351.
15. Smith GI, Shankaran M, Yoshino M, Schweitzer GG, Chondronikola M, Beals JW, Okunade AL, Patterson BW, Nyangau E, Field T, Sirlin CB, Talukdar S, Hellerstein MK, Klein S. Insulin resistance drives hepatic de novo lipogenesis in nonalcoholic fatty liver disease. J Clin Invest 2020;130:1453–1460.
16. Titchenell PM, Lazar MA, Birnbaum MJ. Unraveling the regulation of hepatic metabolism by insulin. Trends Endocrinol Metab 2017;28:497–505.
17. Lambert JE, Parks EJ. Postprandial metabolism of meal triglyceride in humans. Biochim Biophys Acta 2012; 1821:721–726.
18. Syed-Abdul MM, Parks EJ, Gaballah AH, Bingham K, Hammoud GM, Kemble G, Buckley D, McCulloch W, Manrique-Acevedo C. Fatty acid synthase inhibitor TVB-2640 reduces hepatic de novo lipogenesis in males with metabolic abnormalities. Hepatology 2020;72:103–118.
19. Lawitz EJ, Coste A, Poordad F, Alkhouri N, Loo N, McColgan BJ, Tarrant JM, Nguyen T, Han L, Chung C, Ray AS, McHutchison JG, Subramanian GM, Myers RP, Middleton MS, Sirlin C, Loomba R, Nyangau E, Fitch M, Li K, Hellerstein M. Acetyl-CoA carboxylase inhibitor GS-0976 for 12 weeks reduces hepatic de novo lipogenesis and steatosis in patients with nonalcoholic steatohepatitis. Clin Gastroenterol Hepatol 2018;16:1983–1991.e3.
20. Amin NB, Carvajal-Gonzalez S, Purkal J, Zhu T, Crowley C, Perez S, Chidsey K, Kim AM, Goodwin B. Targeting diacylglycerol acyltransferase 2 for the treatment of nonalcoholic steatohepatitis. Sci Transl Med 2019;11:eaav9701.
21. Ratziu V, Harrison SA, Francque S, Bedossa P, Lehert P, Serfaty L, Romero-Gomez M, Boursier J, Abdelmalek M, Caldwell S, Drenth J, Anstee QM, Hum D, Hanf R, Roudot A, Megnien S, Staels B, Sanyal A, Mathurin P,

Gournay J, Nguyen-Khac E, De Ledinghen V, Larrey D, Tran A, Bourliere M, Maynard-Muet M, Asselah T, Henrion J, Nevens F, Cassiman D, Geerts A, Moreno C, Beuers UH, Galle PR, Spengler U, Bugianesi E, Craxi A, Angelico M, Fargion S, Voiculescu M, Gheorghe L, Preotescu L, Caballeria J, Andrade RJ, Crespo J, Callera JL, Ala A, Aithal G, Abouda G, Luketic V, Huang MA, Gordon S, Pockros P, Poordad F, Shores N, Moehlen MW, Bambha K, Clark V, Satapathy S, Parekh S, Reddy RK, Sheikh MY, Szabo G, Vierling J, Foster T, Umpierrez G, Chang C, Box T, Gallegos-Orozco J; GOLDEN-505 Investigator Study Group. Elafibranor, an agonist of the peroxisome proliferator-activated receptor-α and -δ, induces resolution of nonalcoholic steatohepatitis without fibrosis worsening. Gastroenterology 2016;150:1147–1159.e5.

22. Kim CW, Addy C, Kusunoki J, Anderson NN, Deja S, Fu X, Burgess SC, Li C, Chakravarthy M, Previs S, Milstein S, Fitzgerald K, Kelley DE, Horton JD. Acetyl CoA carboxylase inhibition reduces hepatic steatosis but elevates plasma triglycerides in mice and humans: a bedside to bench investigation. Cell Metab 2017; 26:394–406.e6.
23. Ben-Sahra I, Manning BD. mTORC1 signaling and the metabolic control of cell growth. Curr Opin Cell Biol 2017;45:72–82.
24. Sengupta S, Peterson TR, Laplante M, Oh S, Sabatini DM. mTORC1 controls fasting-induced ketogenesis and its modulation by ageing. Nature 2010; 468:1100–1104.
25. Garami A, Zwartkruis FJT, Nobukuni T, Joaquin M, Roccio M, Stocker H, Kozma SC, Hafen E, Bos JL, Thomas G. Insulin activation of Rheb, a mediator of mTOR/S6K/4E-BP signaling, is inhibited by TSC1 and 2. Mol Cell 2003;11:1457–1466.
26. Li S, Brown MS, Goldstein JL. Bifurcation of insulin signaling pathway in rat liver: mTORC1 required for stimulation of lipogenesis, but not inhibition of gluconeogenesis. Proc Natl Acad Sci U S A 2010; 107:3441–3446.
27. Porstmann T, Santos CR, Griffiths B, Cully M, Wu M, Leevers S, Griffiths JR, Chung YL, Schulze A. SREBP activity is regulated by mTORC1 and contributes to Akt-dependent cell growth. Cell Metab 2008;8:224–236.
28. Yecies JL, Zhang HH, Menon S, Liu S, Yecies D, Lipovsky AI, Gorgun C, Kwiatkowski DJ, Hotamisligil GS, Lee CH, Manning BD. Akt stimulates hepatic SREBP1c and lipogenesis through parallel mTORC1-dependent and independent pathways. Cell Metab 2011;14:21–32.
29. Wan M, Leavens KF, Saleh D, Easton RM, Guertin DA, Peterson TR, Kaestner KH, Sabatini DM, Birnbaum MJ. Postprandial hepatic lipid metabolism requires signaling through Akt2 independent of the transcription factors FoxA2, FoxO1, and SREBP1c. Cell Metab 2011; 14:516–527.
30. Titchenell PM, Quinn WJ, Lu M, Chu Q, Lu W, Li C, Chen H, Monks BR, Chen J, Rabinowitz JD, Birnbaum MJ. Direct hepatocyte insulin signaling is required for lipogenesis but is dispensable for the suppression of glucose production. Cell Metab 2016; 23:1154–1166.
31. Kenerson HL, Subramanian S, McIntyre R, Kazami M, Yeung RS. Livers with constitutive mTORC1 activity resist steatosis independent of feedback suppression of akt. PLoS One 2015;10:e0117000.
32. Kenerson HL, Yeh MM, Yeung RS. Tuberous sclerosis complex-1 deficiency attenuates diet-induced hepatic lipid accumulation. PLoS One 2011;6:e18075.
33. Haas ME, Attie AD, Biddinger SB. The regulation of ApoB metabolism by insulin. Trends Endocrinol Metab 2013; 24:391–397.
34. Quinn WJ, Shewale Sv, Wan M, Gelfer R, Rader DJ, Birnbaum MJ, Titchenell PM. mTORC1 stimulates phosphatidylcholine synthesis to promote triglyceride secretion. J Clin Invest 2017;127:4207–4215.
35. Ai D, Baez JM, Jiang H, Conlon DM, Hernandez-Ono A, Frank-Kamenetsky M, Milstein S, Fitzgerald K, Murphy AJ, Woo CW, Strong A, Ginsberg HN, Tabas I, Rader DJ, Tall AR. Activation of ER stress and mTORC1 suppresses hepatic sortilin-1 levels in obese mice. J Clin Invest 2012;122:1677–1687.
36. Umemura A, Park EJ, Taniguchi K, Lee JH, Shalapour S, Valasek MA, Aghajan M, Nakagawa H, Seki E, Hall MN, Karin M. Liver damage, inflammation, and enhanced tumorigenesis after persistent mTORC1 inhibition. Cell Metab 2014;20:133–144.
37. Zhu AX, Kudo M, Assenat E, Cattan S, Kang YK, Lim HY, Poon RTP, Blanc JF, Vogel A, Chen CL, Dorval E, Peck-Radosavljevic M, Santoro A, Daniele B, Furuse J, Jappe A, Perraud K, Anak O, Sellami DB, Chen LT. Effect of everolimus on survival in advanced hepatocellular carcinoma after failure of sorafenib: the EVOLVE-1 randomized clinical trial. JAMA 2014;312:57–67.
38. Fujita K, Nozaki Y, Wada K, Yoneda M, Fujimoto Y, Fujitake M, Endo H, Takahashi H, Inamori M, Kobayashi N, Kirikoshi H, Kubota K, Saito S, Nakajima A. Dysfunctional very-low-density lipoprotein synthesis and release is a key factor in nonalcoholic steatohepatitis pathogenesis. Hepatology 2009;50:772–780.
39. Tremblay F, Brûlé S, Sung HU, Li Y, Masuda K, Roden M, Xiao JS, Krebs M, Polakiewicz RD, Thomas G, Marette A. Identification of IRS-1 Ser-1101 as a target of S6K1 in nutrient- and obesity-induced insulin resistance. Proc Natl Acad Sci U S A 2007;104:14056–14061.
40. Khamzina L, Veilleux A, Bergeron S, Marette A. Increased activation of the mammalian target of rapamycin pathway in liver and skeletal muscle of obese rats: possible involvement in obesity-linked insulin resistance. Endocrinology 2005;146:1473–1481.
41. Leclercq IA, Farrell GC, Schriemer R, Robertson GR. Leptin is essential for the hepatic fibrogenic response to chronic liver injury. J Hepatol 2002;37:206–213.
42. Matsumoto M, Hada N, Sakamaki Y, Uno A, Shiga T, Tanaka C, Ito T, Katsume A, Sudoh M. An improved mouse model that rapidly develops fibrosis in non-alcoholic steatohepatitis. Int J Exp Pathol 2013; 94:93–103.
43. Chiba T, Suzuki S, Sato Y, Itoh T, Umegaki K. Evaluation of methionine content in a high-fat and choline-deficient

diet on body weight gain and the development of non-alcoholic steatohepatitis in mice. PLoS One 2016;11:e0164191.
44. Zhao P, Sun X, Chaggan C, Liao Z, Wong K, He F, Singh S, Loomba R, Karin M, Witztum JL, Saltiel AR. An AMPK–caspase-6 axis controls liver damage in nonalcoholic steatohepatitis. Science 2020;367:652–660.
45. Roth JD, Dolman CS, Clapper JR, Heilig JS, Villescaz C, Athanacio J, Herich J, Ghosh SS, Hendricks MD, Gu G, Wittmer C, Lowe C. Diet-induced mouse model of fatty liver disease and nonalcoholic steatohepatitis reflecting clinical disease progression and methods of assessment. Am J Physiol Gastrointest Liver Physiol 2013;305:G483–G495.
46. Huang J, Manning BD. A complex interplay between Akt, TSC2 and the two mTOR complexes. Biochemi Soc Transact 2009;37:217–222.
47. Millar JS, Cromley DA, McCoy MG, Rader DJ, Billheimer JT. Determining hepatic triglyceride production in mice: comparison of poloxamer 407 with Triton WR-1339. J Lipid Res 2005;46:2023–2028.
48. Jacobs RL, Lingrell S, Zhao Y, Francis GA, Vance DE. Hepatic CTP:phosphocholine cytidylyltransferase-α is a critical predictor of plasma high density lipoprotein and very low density lipoprotein. J Biol Chem 2008;283:2147–2155.
49. Li Z, Agellon LB, Allen TM, Umeda M, Jewell L, Mason A, Vance DE. The ratio of phosphatidylcholine to phosphatidylethanolamine influences membrane integrity and steatohepatitis. Cell Metab 2006;3:321–331.
50. Niebergall LJ, Jacobs RL, Chaba T, Vance DE. Phosphatidylcholine protects against steatosis in mice but not non-alcoholic steatohepatitis. Biochim Biophys Acta 2011;1811:1177–1185.
51. Puri P, Baillie RA, Wiest MM, Mirshahi F, Choudhury J, Cheung O, Sargeant C, Contos MJ, Sanyal AJ. A lipidomic analysis of nonalcoholic fatty liver disease. Hepatology 2007;46:1081–1090.
52. Kennedy EP, Weiss SB. The function of cytidine coenzyme in the biosynthesis of phospholipides. J Biol Chem 1956;222:193–214.
53. Jacobs RL, Devlin C, Tabas I, Vance DE. Targeted deletion of hepatic CTP:phosphocholine cytidylyltransferase α in mice decreases plasma high density and very low density lipoproteins. J Biol Chem 2004;279:47402–47410.
54. Luukkonen PK, Tukiainen T, Juuti A, Sammalkorpi H, Nidhina Haridas PA, Niemelä O, Arola J, Orho-Melander M, Hakkarainen A, Kovanen PT, Dwivedi O, Groop L, Hodson L, Gastaldelli A, Hyötyläinen T, Orešič M, Yki-Järvinen H. Hydroxysteroid 17-β dehydrogenase 13 variant increases phospholipids and protects against fibrosis in nonalcoholic fatty liver disease. JCI Insight 2020;5:e132158.
55. Pirola CJ, Garaycoechea M, Flichman D, Arrese M, Martino JS, Gazzi C, Castaño GO, Sookoian S. Splice variant rs72613567 prevents worst histologic outcomes in patients with nonalcoholic fatty liver disease. J Lipid Res 2019;60:176–185.
56. Ono H, Shimano H, Katagiri R, Yahagi N, Sakoda H, Onishi Y, Anai M, Ogihara T, Fujishiro M, Viana AYI, Fukushima Y, Abe M, Shojima N, Kikuchi M, Yamada N, Oka Y, Asano T. Hepatic Akt activation induces marked hypoglycemia, hepatomegaly, and hypertriglyceridemia with sterol regulatory element binding protein involvement. Diabetes 2003;52:2905–2913.
57. Haeusler RA, Hartil K, Vaitheesvaran B, Arrieta-Cruz I, Knight CM, Cook JR, Kammoun HL, Febbraio MA, Gutierrez-Juarez R, Kurland IJ, Accili D. Integrated control of hepatic lipogenesis versus glucose production requires FoxO transcription factors. Nat Comm 2014;5:5190.
58. Brunet A, Bonni A, Zigmond MJ, Lin MZ, Juo P, Hu LS, Anderson MJ, Arden KC, Blenis J, Greenberg ME. Akt promotes cell survival by phosphorylating and inhibiting a forkhead transcription factor. Cell 1999;96:857–868.
59. Foretz M, Pacot C, Dugail I, Lemarchand P, Guichard C, le Lièpvre X, Berthelier-Lubrano C, Spiegelman B, Kim JB, Ferré P, Foufelle F. ADD1/SREBP-1c is required in the activation of hepatic lipogenic gene expression by glucose. Mol Cell Biol 2015;19:3760–3768.
60. Zhang W, Patil S, Chauhan B, Guo S, Powell DR, Le J, Klotsas A, Matika R, Xiao X, Franks R, Heidenreich KA, Sajan MP, Farese RV, Stolz DB, Tso P, Koo SH, Montminy M, Unterman TG. FoxO1 regulates multiple metabolic pathways in the liver effects on gluconeogenic, glycolytic, and lipogenic gene expression. J Biol Chem 2006;281:10105–10117.
61. Sakai J, Nohturfft A, Goldstein JL, Brown MS. Cleavage of sterol regulatory element-binding proteins (SREBPs) at site-1 requires interaction with SREBP cleavage-activating protein. J Biol Chem 2002;273:5785–5793.
62. Hua X, Nohturfft A, Goldstein JL, Brown MS. Sterol resistance in CHO cells traced to point mutation in SREBP cleavage–activating protein xianxin. Cell 1996;87:415–426.
63. Papazyan R, Sun Z, Kim YH, Titchenell PM, Hill DA, Lu W, Damle M, Wan M, Zhang Y, Briggs ER, Rabinowitz JD, Lazar MA. Physiological suppression of lipotoxic liver damage by complementary actions of HDAC3 and SCAP/SREBP. Cell Metab 2016;24:863–874.
64. Okuno T, Kakehashi A, Ishii N, Fujioka M, Gi M, Wanibuchi H. mTOR activation in liver tumors is associated with metabolic syndrome and non-alcoholic steatohepatitis in both mouse models and humans. Cancers (Basel) 2018;10:465.
65. Düvel K, Yecies JL, Menon S, Raman P, Lipovsky AI, Souza AL, Triantafellow E, Ma Q, Gorski R, Cleaver S, Vander Heiden MG, MacKeigan JP, Finan PM, Clish CB, Murphy LO, Manning BD. Activation of a metabolic gene regulatory network downstream of mTOR complex 1. Mol Cell 2010;39:171–183.
66. Li S, Ogawa W, Emi A, Hayashi K, Senga Y, Nomura K, Hara K, Yu D, Kasuga M. Role of S6K1 in regulation of SREBP1c expression in the liver. Biochem Biophys Res Comm 2011;412:197–202.
67. Harrington LS, Findlay GM, Gray A, Tolkacheva T, Wigfield S, Rebholz H, Barnett J, Leslie NR, Cheng S,

Shepherd PR, Gout I, Downes CP, Lamb RF. The TSC1-2 tumor suppressor controls insulin-PI3K signaling via regulation of IRS proteins. J Cell Biol 2004;166:213–223.
68. Shah OJ, Wang Z, Hunter T. Inappropriate activation of the TSC/Rheb/mTOR/S6K cassette induces IRS1/2 depletion, insulin resistance, and cell survival deficiencies. Curr Biol 2004;14:1650–1656.
69. Guertin DA, Stevens DM, Thoreen CC, Burds AA, Kalaany NY, Moffat J, Brown M, Fitzgerald KJ, Sabatini DM. Ablation in mice of the mTORC components raptor, rictor, or mLST8 reveals that mTORC2 is required for signaling to Akt-FOXO and PKCα, but Not S6K1. Dev Cell 2006;11:859–871.
70. O'Doherty RM, Lehman DL, Télémaque-Potts S, Newgard CB. Metabolic impact of glucokinase overexpression in liver: lowering of blood glucose in fed rats is accompanied by hyperlipidemia. Diabetes 1999; 48:2022–2027.
71. Yao Z, Vance DE. The active synthesis of phosphatidylcholine is required for very low density lipoprotein secretion from rat hepatocytes. J Biol Chem 1988; 263:2998–3004.
72. Buchman AL, Dubin MD, Moukarzel AA, Jenden DJ, Roch M, Rice KM, Gornbein J, Ament ME. Choline deficiency: a cause of hepatic steatosis during parenteral nutrition that can be reversed with intravenous choline supplementation. Hepatology 1995;22:1399–1403.
73. Schneider CV, Markus K, Conlon DM, Strnad P, Christoph A, Rader DJ. A genome-first approach to mortality and metabolic phenotypes in MTARC1 homozygotes. Med (NY) 2021;2:851–863.e3.
74. Luukkonen PK, Juuti A, Sammalkorpi H, Penttilä AK, Orešič M, Hyötyläinen T, Arola J, Orho-Melander M, Yki-Järvinen H. MARC1 variant rs2642438 increases hepatic phosphatidylcholines and decreases severity of nonalcoholic fatty liver disease in humans. J Hepatol 2020; 73:725–726.
75. Luukkonen PK, Nick A, Hölttä-Vuori M, Thiele C, Isokuortti E, Lallukka-Brück S, Zhou Y, Hakkarainen A, Lundbom N, Peltonen M, Orho-Melander M, Orešič M, Hyötyläinen T, Hodson L, Ikonen E, Yki-Järvinen H. Human PNPLA3-I148M variant increases hepatic retention of polyunsaturated fatty acids. JCI Insight 2019;4: e127902.
76. Ehrhardt N, Doche ME, Chen S, Mao HZ, Walsh MT, Bedoya C, Guindi M, Xiong W, Ignatius Irudayam J, Iqbal J, Fuchs S, French SW, Mahmood Hussain M, Arditi M, Arumugaswami V, Péterfy M. Hepatic Tm6sf2 overexpression affects cellular ApoB-trafficking, plasma lipid levels, hepatic steatosis and atherosclerosis. Hum Mol Gen 2017;26:2719–2731.
77. Trépo E, Romeo S, Zucman-Rossi J, Nahon P. PNPLA3 gene in liver diseases. J Hepatol 2016;65:399–412.
78. Luukkonen PK, Zhou Y, Haridas N, Dwivedi OP, Hyötyläinen T, Ali A, Juuti A, Leivonen M, Tukiainen T, Ahonen L, Scott E, Palmer JM, Arola J, Orho-Melander M, Vikman P, Anstee QM, Olkkonen VM, Orešič M, Groop L, Yki-Järvinen H. Impaired hepatic lipid synthesis from polyunsaturated fatty acids in TM6SF2 E167K variant carriers with NAFLD. J Hepatol 2017; 67:128–136.
79. Kozlitina J, Smagris E, Stender S, Nordestgaard BG, Zhou HH, Tybjærg-Hansen A, Vogt TF, Hobbs HH, Cohen JC. Exome-wide association study identifies a TM6SF2 variant that confers susceptibility to nonalcoholic fatty liver disease. Nat Genet 2014;46:352–356.
80. Dai D, Wen F, Zhou S, Su Z, Liu G, Wang M, Zhou J, He F. Association of MTTP gene variants with pediatric NAFLD: a candidate-gene-based analysis of single nucleotide variations in obese children. PLoS One 2017; 12:e0185396.
81. Hsiao PJ, Lee MY, Wang YT, Jiang HJ, Lin PC, Yang YHC, Kuo KK. MTTP-297H polymorphism reduced serum cholesterol but increased risk of non-alcoholic fatty liver disease-a cross-sectional study. BMC Med Genet 2015;16:19.
82. Lonardo A, Nascimbeni F, Mantovani A, Targher G. Hypertension, diabetes, atherosclerosis and NASH: cause or consequence? J Hepatol 2018;68:335–352.
83. Bronson RT, Manning BD, Nicholatos J, Menon S, Yecies JL, Zhang HH, Harputlugil E, Kwiatkowski DJ, Howell JJ. Chronic activation of mTOR complex 1 is sufficient to cause hepatocellular carcinoma in mice. Sci Signal 2012;5:ra24.
84. Matsumoto M, Pocai A, Rossetti L, DePinho RA, Accili D. Impaired regulation of hepatic glucose production in mice lacking the forkhead transcription factor Foxo1 in liver. Cell Metab 2007;6:208–216.
85. Folch J, Lees M, Sloane Stanley G. A simple method for the isolation and purification of total lipides from animal tissues. J Biol Chem 1957;226:497–509.
86. Abreu S, Solgadi A, Chaminade P. Optimization of normal phase chromatographic conditions for lipid analysis and comparison of associated detection techniques. J Chromatogr A 2017;1514:54–71.
87. Lian J, van der Veen JN, Watts R, Jacobs RL, Lehner R. Carboxylesterase 1d (Ces1d) does not contribute to cholesteryl ester hydrolysis in the liver. J Lipid Res 2021; 62:100093.
88. Leavens KF, Easton RM, Shulman GI, Previs SF, Birnbaum MJ. Akt2 is required for hepatic lipid accumulation in models of insulin resistance. Cell Metab 2009;10:405–418.
89. Kleiner DE, Brunt EM, van Natta M, Behling C, Contos MJ, Cummings OW, Ferrell LD, Liu YC, Torbenson MS, Unalp-Arida A, Yeh M, McCullough AJ, Sanyal AJ; Nonalcoholic Steatohepatitis Clinical Research Network. Design and validation of a histological scoring system for nonalcoholic fatty liver disease. Hepatology 2005;41:1313–1321.

Received December 6, 2021. Accepted February 17, 2022.

Correspondence
Address correspondence to: Paul M. Titchenell, PhD, 3400 Civic Center Blvd, Philadelphia, PA 19104. e-mail: ptitc@pennmedicine.upenn.edu; tel: (215) 573-1872.

Acknowledgment
The authors thank Lan Cheng for her expert tissue processing and histology. The authors also thank Dr Mitchell Lazar for providing the AAV8-TBG-nSREBP1c virus.

The authors also acknowledge support from the Mouse Metabolic Phenotyping Core, Penn Vector Core, Penn Diabetes Research Center (P30-DK19525), and the Penn Center for Molecular Studies in Digestive and Liver Diseases (P30-DK050306). Lastly, the authors thank Dr William Quinn, III and all the members of the Titchenell lab for the thoughtful discussions on this project.

CRediT Authorship Contributions

Kahealani Uehara (Conceptualization: Lead; Formal analysis: Lead; Funding acquisition: Lead; Writing – original draft: Lead; Writing – review & editing: Lead)

Jaimarie Sostre-Colón (Methodology: Supporting; Writing – review & editing: Supporting)

Matthew Gavin (Formal analysis: Supporting; Methodology: Supporting)

Dominic Santoleri (Investigation: Supporting; Writing – review & editing: Supporting)

Kelly-Ann Leonard (Data curation: Supporting; Formal analysis: Supporting)

René L. Jacobs (Data curation: Supporting; Formal analysis: Supporting; Methodology: Supporting; Writing – review & editing: Supporting)

Paul Titchenell, PhD (Conceptualization: Lead; Data curation: Lead; Formal analysis: Lead; Funding acquisition: Lead; Investigation: Lead; Methodology: Lead; Project administration: Lead; Supervision: Lead; Writing – original draft: Lead; Writing – review & editing: Lead)

Conflicts of interest

The authors disclose no conflicts.

Funding

This work was supported by United States National Institutes of Health grants R01-DK125497, P30-DK050306, McCabe Fund Fellow Award (Paul M. Titchenell), start-up funds from the University of Pennsylvania (Paul M. Titchenell), the Cox Research Institute (Paul M. Titchenell), United States National Institutes of Health training grant T32-AR053461 and National Research Service Award F31-DK128876 (Kahealani Uehara), and by the Canadian Institutes of Health Research Grant 156243 (René L. Jacobs).